Title: Ice Shell Structure and Composition of Ocean Worlds: Insights from Accreted Ice on Earth

Authors: Natalie S. Wolfenbarger[†], Jacob J. Buffo[‡], Krista M. Soderlund[†], Donald D. Blankenship[†]

[†]Institute for Geophysics, University of Texas at Austin, Austin, TX
[‡]Dartmouth College, Hanover, NH

Corresponding Author:

Natalie S. Wolfenbarger
J.J. Pickle Research Campus
University of Texas Institute for Geophysics
10100 Burnet Road
Austin, TX, 78759-8500, USA
nwolfenb@utexas.edu

Running Title: Ice Shell Structure and Composition of Ocean Worlds

Keywords: ocean worlds, ice shell, marine ice, sea ice, fractionation, salinity

Abstract: Accreted ice retains and preserves traces of the ocean from which it formed. In this work we study two classes of accreted ice found on Earth—frazil ice, which forms through crystallization within a supercooled water column, and congelation ice, which forms through directional freezing at an existing interface—and discuss where each might be found in the ice shells of ocean worlds. We focus our study on terrestrial ice formed in low temperature gradient environments (e.g., beneath ice shelves), consistent with conditions expected at the ice-ocean interfaces of Europa and Enceladus and highlight the juxtaposition of compositional trends in relation to ice formed in higher temperature gradient environments (e.g., at the ocean surface). Observations from Antarctic sub-ice-shelf congelation and frazil ice show that the purity of frazil ice can approach two orders of magnitude higher than congelation ice formed in the same low temperature gradient environment (~0.1% vs. ~10% of the ocean salinity). Studies of fractionation in sea ice and marine ice suggest the fractionation of major ionic species will be minor but should broadly scale with ion diffusivity. In addition, where congelation ice can maintain a planar ice-water interface on a microstructural scale, forming "lake ice", the efficiency of salt rejection is enhanced (~1% of the ocean salinity) and lattice soluble impurities such as chloride are preferentially incorporated. We conclude that an ice shell which forms by gradual thickening as its interior cools would be composed of congelation ice, whereas frazil ice will form where the ice shell thins on local (rifts and basal fractures) or regional (latitudinal gradients) scales through the operation of an "ice pump".

1. **Introduction**

The ice shells of ocean worlds govern the feasibility of surface-ice-ocean exchange, thought to be significant for supporting habitats within the sub-ice oceans (Peddinti and McNamara 2015; Soderlund *et al.* 2020; Vance *et al.* 2016; Vance *et al.* 2018). The dynamic features and young surfaces of Europa and Enceladus provide compelling evidence that their subsurface oceans are continuously interacting with their overlying ice shells (Howell and Pappalardo 2018; Manga and Wang 2007; O'Neill and Nimmo 2010; Pappalardo and Barr 2004; Spencer *et al.* 2018; Thomas *et al.* 2016). Because existing observations are mostly confined to the surface, much attention has been directed towards the properties of the uppermost layer of the ice shell, where the native ice could be modified by exogenic processes (Brown and Hand 2013). Although observations of the surface provide important constraints on processes operating in the subsurface (Zolotov and Shock 2001), the properties of the subsurface itself have received less focus. Processes occurring at the ice-ocean interface, such as accretion, are likely responsible for governing and modulating bulk properties of the ice shell (Buffo *et al.* 2020; Kargel *et al.* 2000; Pappalardo and Barr 2004; Peddinti and McNamara 2015; Zolotov and Shock 2001). Ice formed from the freezing of ocean water, referred to here as accreted ice, can serve as a fingerprint of the ocean below, recording signals of circulation (Langhorne and Robinson 1986; Souchez *et al.* 2004), composition and salinity (Petrich and Eicken 2017; Souchez *et al.* 1991), and potentially life (Martin and McMinn 2018; Roberts *et al.* 2006).

The ice-ocean interfaces of these alien worlds and the processes that mold and shape them are not unlike those found in Earth's cryosphere. The accretion of ice at an ice-ocean interface has been the subject of significant study because of its relevance to engineering (Timco and Weeks 2010), climate (Vihma 2014), and biology (Arrigo 2014). This extensive research represents a foundation from which to build an understanding of ice on other worlds. Previous work has leveraged sea ice as an analog to interpret surface features and connect them to processes that may be operating within Europa's ice shell (Greeley *et al.* 1998), yet these authors advised caution in drawing direct analogies between the Earth and Europa given their distinct environmental conditions (i.e., rapidly forming, seasonal ice on Earth versus deep ice that has formed over thousands to millions of years on icy worlds). Many recent works have revisited terrestrial analogs to improve our understanding of potential ice-ocean interactions on other worlds (e.g., Buffo *et al.* 2020; Schmidt 2020; Soderlund *et al.* 2020). Still, existing publications have leveraged only a small fraction of this vast and relatively untapped resource.

In this work we demonstrate that terrestrial accreted ice can serve as a relevant analog for the ice shells of ocean worlds, particularly Europa and Enceladus (Section 2). We present two fundamental classes of accreted ice analogs: frazil ice and congelation ice (Section 3) and examine how their formation mechanisms influence bulk ice salinity at low temperature gradients (Section 4). We identify terrestrial analogs for accreted ice on icy ocean worlds (Section 5), highlighting the implications for geophysical processes, chemistry, astrobiology, the entrainment of biosignatures, and remote sensing (Section 6).

2. **Physico-chemical environments of Europa and Enceladus**

The exotic appearances of the ice shells of ocean worlds can sometimes mask the more mundane reality that they are primarily composed of hexagonal water ice, the dominant ice on Earth. Furthermore, at the ice-ocean interface, where accretion of ice occurs, the physical conditions (e.g., composition, salinity, temperature, pressure) could be similar to those found in Earth's polar regions. Table 1 depicts the observational and modeled constraints on the conditions at the ice-ocean interfaces of Europa and Enceladus and demonstrates their similarity to Earth.

TABLE 1. Constraints on the conditions at the ice-ocean interfaces of Earth, Europa, and Enceladus from observations and models. The estimates of ice thickness for Europa refer to estimates from crater and thermodynamic analyses from Billings and Kattenhorn (2005). The pressure and temperature estimates are derived from the ice thickness ranges presented here and assume pure water ice at a density of 917 kg/m^3 and a freshwater ocean.

Parameter	Europa	Enceladus	Earth	References
Composition (Dominant Ions)	Mg^{2+}, SO_4^{2-}, Na^+, Cl^-	Na^+, Cl^-, HCO_3^-, CO_3^{2-}	Cl^-, Na^+, Mg^{2+}, SO_4^{2-}	Fox-Powell and Cousins (2021); Glein *et al.* (2018); Glein *et al.* (2015); Postberg *et al.* (2018); Zolotov (2007); Zolotov and Shock (2001)
Salinity (Constrained by Geochemical Models)	12.3 g/kg	2−20 g/kg	N/A	Zolotov (2007); Zolotov and Shock (2001)
Salinity (Constrained by Observation)	>5 ppt	5−20 ppt	35 ppt	Postberg *et al.* (2011); Schilling *et al.* (2007)
Floating Ice Thickness	3−38 km	2−50 km	0−3 km	Billings and Kattenhorn (2005); (Čadek *et al.* 2019); Čadek *et al.* (2016); Iess *et al.* (2014); McKinnon (2015)
Pressure	3.6−46 MPa	0.2−5.2 MPa	0.1−5.6 MPa	
Pressure-Melting Temperature	269−273 K	273 K	270−273 K	

The composition and salinity of accreted ice serves as a signature of the environment in which it formed (Buffo *et al.* 2020; Zolotov and Kargel 2009). Although the compositions of the subsurface oceans on Europa and Enceladus have not been measured directly, constraints exist from theory and interpretations of data collected by both space-based and Earth-based platforms (e.g., Postberg *et al.* 2011; Zolotov and Shock 2001). Because the composition of the source water influences the properties of the ice (i.e., phase behavior governs brine volume fraction which influences thermophysical, dielectric, and mechanical properties) (Petrich and Eicken 2017), it should be considered when evaluating the relevance of terrestrial accreted ice as an analog.

Measurements of the Enceladus plume material by *Cassini* represents the only in situ observation of apparent oceanic material in the outer solar system (Glein *et al.* 2018), although atmospheric gasses measured by the *Huygens* probe on Titan, another icy ocean moon in the Saturnian system, could have contributions from outgassed oceanic material (Tobie *et al.* 2012). These observations, coupled with geochemical models (Glein *et al.* 2015; Zolotov 2007), suggest that the Enceladan ocean is highly alkaline and dominantly composed of sodium and chloride (Glein *et al.* 2018; Postberg *et al.* 2018). Assuming the plume material represents a relatively unfractionated (i.e., flash-frozen) sample of oceanic material (Fox-Powell and Cousins 2021), the salinity of the Enceladan ocean could be up to ~20 ppt—only slightly less than Earth's (~35 ppt) (Postberg et al., 2011).

Although a plume sample remains elusive for Europa, models of Europa's ocean chemistry have been tuned by Earth-based observations of chemical species detected in Europa's tenuous atmosphere (Brown 2001; Zolotov and Shock 2001). These models suggest that Europa's ocean composition is broadly comparable to that of the Earth's, where the dominant ionic species are chloride, sodium, magnesium, and sulfate. Early interpretations of *Galileo* NIMS data were consistent with the presence of hydrated sulfate or carbonate salts in regions associated with resurfacing (McCord *et al.* 1998; McCord *et al.* 1999). Later analysis by Carlson *et al.* (2005) suggested that the signature could instead be attributed to hydrated sulfuric acid. This would also explain the apparent enhancement observed on the trailing hemisphere, where the surface is highly irradiated and bombarded by Iogenic sulfur. Higher spectral resolution observations acquired by Earth-based platforms were able to identify features associated with magnesium sulfate salts but found that they were confined to the trailing hemisphere and spatially correlated with sulfuric acid (Brown and Hand 2013). Brown and Hand (2013) used the spatial correlation of the magnesium sulfate with radiation products to argue that sulfate salts are a radiation product and that the ice shell and ocean are dominantly composed of chloride salts, which have no distinct spectral feature in the near-infrared. These results were supported by additional Earth-based observations, which were able to confirm that acid-dominant components were concentrated along the trailing hemisphere and salt-dominant components were associated with endogenous surface features (Fischer *et al.* 2015). Additionally, because the salt-dominant component lacked spectral features consistent with hydrated sulfate minerals, the authors proposed the spectrum may instead be associated with chloride evaporite deposits. Laboratory experiments have demonstrated that when sodium chloride is exposed to conditions similar to those expected at Europa's surface, it darkens into a color consistent with that observed across Europa's surface, particularly in features thought to be associated with material from the sub-ice ocean (Hand and Carlson 2015). Recent observations of Europa's surface with the *Hubble Space Telescope* revealed a spectral feature consistent with irradiated sodium chloride that was again highly correlated with endogenous features (Trumbo *et al.* 2019). These laboratory, Earth-based, and space-based observations collectively indicate that chloride salts are being entrained in the ice shell. Similar to the Earth and Enceladus, chloride may represent an important component of Europa's ocean composition.

Although measurements of Europa's induced magnetic field by the *Galileo* magnetometer supports the existence of a global subsurface ocean; constraining the salinity of the ocean from these measurements is a challenge as the signal is a convolution of electrical conductivity and ice/ocean thicknesses. Gravitational measurements from *Galileo* flybys provide an upper limit of ~200 km to the thickness of the ice/ocean layer (Anderson *et al.* 1998). Using this thickness constraint and a minimum value of 0.7 for the normalized amplitude of the induced dipole moment relative to the primary field, Zimmer *et al.* (2000) were able to estimate a minimum ocean conductivity of 0.072 S/m. Later work by Schilling *et al.* (2007) further constrained the parameter space to obtain a minimum conductivity of 0.5 S/m for a 100 km ocean. For terrestrial seawater at 0 °C, this translates to a practical salinity (PSS-78) of ~5. Hand and Chyba (2007) use the induced magnetic field amplitude of 0.97 obtained by Schilling *et al.* (2004) to argue for a thin ice shell (less than 15 km thick) overlying an ocean of conductivity that could range from 3 S/m (practical salinity of ~36 at 0 °C) to 23 S/m (practical salinity undefined, exceeds upper limit of conductivity for saturated NaCl and $MgSO_4$ aqueous solutions presented by Hand and Chyba (2007)). This suggests, because of the broad parameter space of possible ocean salinities, a valid ocean analog could span in salinity from brackish to hypersaline.

The surfaces of icy ocean worlds are directly exposed to the vacuum of space and have measured temperatures ranging from approximately 86 K to 132 K on Europa (Spencer et al., 1999) and 32 K up to 145 K on Enceladus (Spencer *et al.* 2006). At the south pole of Enceladus, the temperature approaches 200 K near a set of linear features, referred to as tiger stripes, which are spatially correlated with the plumes observed by *Cassini* and are thought to serve as a conduit to the subsurface ocean (Hemingway *et al.* 2020; Spencer *et al.* 2018). The conditions at depth, however, could be relatively mild. The equivalent of one Earth atmosphere of pressure translates to ~100 m of ice on Europa and ~1 km of ice on Enceladus (Fig. 1a). This suggests the near-vacuum conditions at the surface of these bodies becomes irrelevant at relatively shallow depths, well-below the hypothesized ice shell thicknesses of Europa and Enceladus (Table 1). The pressure ranges expected beneath these ice shells are consistent with what is expected beneath floating ice on Earth, which can be up to a few kilometers thick (Table 1, Fig. 1). The melting temperature of ice does not vary significantly with pressure for ice shell thicknesses of approximately 1 m to a few kilometers on Europa and 10 m to tens of kilometers on Enceladus. This suggests that for both Europa and Enceladus, neglecting the influence of impurities, the temperature at the ice-ocean interface is likely to be depressed by only a few degrees (~3 K beneath a 30 km ice shell on Europa, ~0.5 K beneath a 50 km ice shell on Enceladus). Note that although the influence of pressure on melting temperature is minor, it is critical to driving “ice pumps” beneath ice shelves on Earth, a basal ice redistribution process introduced and further discussed in Section 3.2. The pressure-melting temperature represents an upper limit for the temperature at the ice-ocean interface since impurities within the ocean can further reduce the equilibrium temperature.

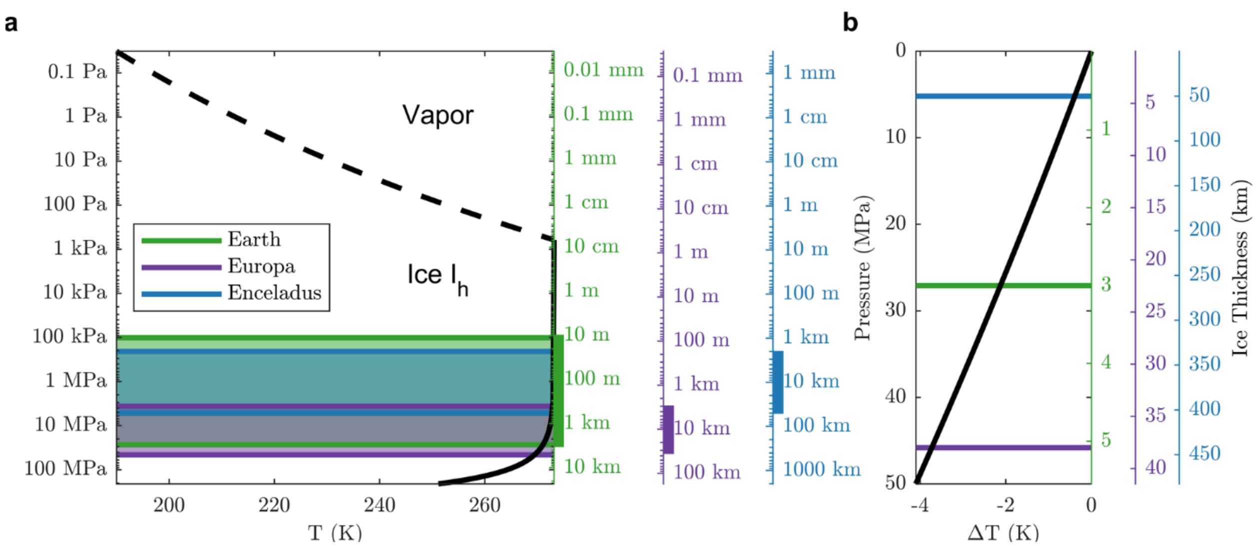

FIG. 1. Pressure at the ice-ocean interface for the range of ice shell thicknesses on Earth (green axis), Europa (purple axis), and Enceladus (blue axis) represented **(a)** logarithmically across the entire stable region of ice Ih and **(b)** linearly across the range of pressures expected at the ice-ocean interfaces of these worlds. The Earth axis does not include the effect of atmospheric pressure, hence the minimum pressure-equivalent thickness of 10 m. This has minimal effect on the pressure-equivalent ice thickness above atmospheric pressure (101,325 Pa). The dashed black curve depicts the phase boundary between Ice Ih and water vapor, and the solid black curve depicts the phase boundary between Ice Ih and liquid water. The range of floating ice thickness for each body, specified in Table 1, is represented by the shaded region in (a). The colored lines depict the upper and lower bounds of ice thickness. Only the upper bound ice thickness is included in (b). The density of ice is taken to be constant at 917 kg/m^3.

Freezing point depression is a mechanism often invoked to explain the presence of liquid water in otherwise cryogenic environments (Hammond *et al.* 2018; Toner *et al.* 2014). For an ideal solution with low concentrations of impurities, freezing point depression is dependent upon the concentration of dissolved impurities, but not their composition, and is represented by a relationship known as Blagden's law. As the eutectic point is approached, this colligative assumption breaks down and composition becomes relevant to the freezing point depression. For the range of plausible salinities and ice shell thicknesses hypothesized for Europa, this implies the temperature at the ice-ocean interface could range from the pressure-melting point to the eutectic point of a salt solution. For a sodium chloride ocean, the maximum freezing point depression would be ~21 K at a concentration of 232 ppt (Drebushchak *et al.* 2019), whereas for a magnesium sulfate ocean, the maximum corresponds to only ~4 K at a concentration of 174 ppt (Pillay *et al.* 2005). Ammonia, initially implicated in promoting resurfacing processes at Enceladus (Squyres *et al.* 1983), can depress the freezing point of water by almost 100 K at a concentration of 354 ppt (Leliwa-Kopystyński *et al.* 2002); however, only trace amounts were detected in the Enceladus plume material (Waite *et al.* 2009). If the plume observation is representative of the concentration of ammonia within the subsurface ocean, it would amount to a freezing point depression of less than a degree. For outer solar system bodies, such as Triton or Charon, the abundance of ammonia may be more significant (Hammond et al. 2018). The composition and concentration of impurities, in addition to the overburden pressure, defines where multiphase systems can exist within the ice shell (Hammond *et al.* 2018)—creating the opportunity for complex reactive transport processes important to the habitability of these worlds (Buffo *et al.* 2020; Hesse *et al.* 2020; Kalousová *et al.* 2014).

3. **Terrestrial Accreted Ice**

Natural ice is often classified using terminology that is genetic (how it forms) or textural (how it looks). We introduce two classes of accreted ice, consistent with genetic terms used by Tison *et al.* (1998): frazil and congelation. We then present specific terminology used to describe types of accreted ice found on Earth and discuss their relation to each formation mechanism (Fig. 2). Natural accreted ice is rarely composed entirely of frazil or congelation ice, but these broad classifications facilitate discussions of bulk ice properties.

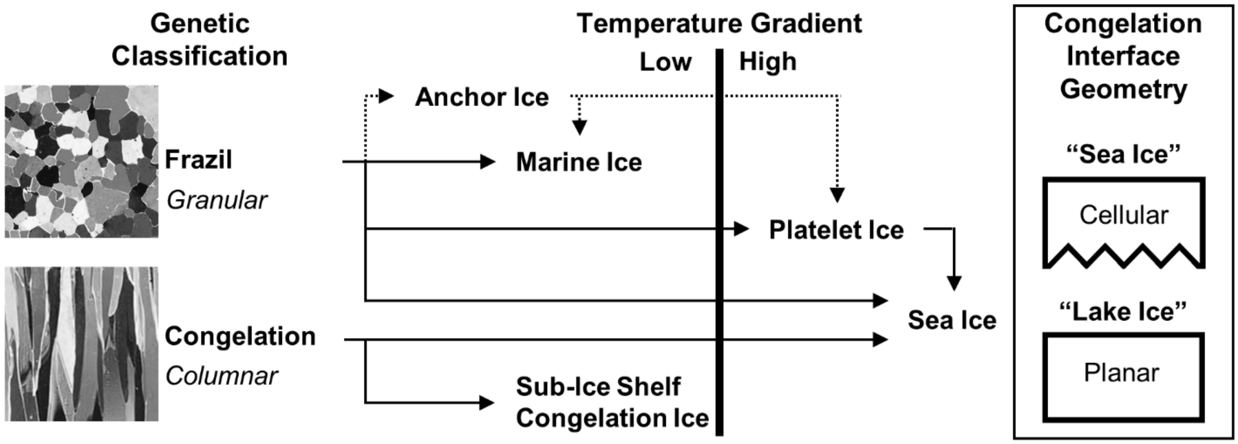

FIG. 2. Genetic classification of accreted ice and terrestrial examples. The italicized text describes the texture associated with each classification of ice. The images depict examples of a granular (USGS 2000) and columnar (Gow and Langston 1977) ice texture. The solid black bar separates low and high temperature gradient accreted ice. The descriptions of the ice-water interface geometry for congelation ice reflect environments where they are generally encountered. The dashed line represents a possible pathway for the formation of platelet or marine ice through the formation of anchor ice (Mager *et al.* 2013).

3.1. Classification of Accreted Ice

Ice that crystallizes within a supercooled water column, as opposed to at an interface, is referred to as frazil ice. Frazil ice is formed in the presence of turbulent water which has been supercooled by tenths to hundredths of a degree (Mager *et al.* 2013; Robinson *et al.* 2019; Weeks and Ackley 1986), where increased supercooling generally promotes increased frazil production (Ettema *et al.* 1984). There are a number of mechanisms in nature that can promote supercooling and thus the production of frazil. Examples of such mechanisms include the adiabatic rise of water masses to a lower-pressure environment and double diffusion occurring between two adjacent water bodies at different temperatures and salinities (see Mager *et al.* 2013). Ice crystals formed from collisions of larger ice crystals, the refreezing of spray, or snow can serve as nucleation sites for frazil ice crystals (Osterkamp 1977). It was long believed that foreign particles, such as organic matter, could serve as nucleation sites for frazil, but no experimental or field observations have demonstrated this is possible at degrees of supercooling observed in nature (<1 °C) (Daly 1984; Robinson *et al.* 2019). Turbulence is also necessary to promote secondary nucleation, responsible for generating meaningful quantities of frazil crystals (Ettema *et al.* 1984). Because frazil ice forms from the accumulation and consolidation of individual crystals which can nucleate independent of each other, it has no preferred orientation and a granular texture (Fig. 2). Post-genetic deformation, caused by sub-ice currents, can alter the texture and result in a banded appearance (Tison *et al.* 1993). Once a stable ice layer has formed, congelation ice growth can occur.

Congelation ice refers to ice produced by the direct freezing of water at an existing ice interface, driven by conductive heat losses (Weeks and Ackley 1986). Congelation ice is characterized by a columnar texture (Fig. 2), where crystals preferentially elongate parallel to the direction of the temperature gradient (Harrison and Tiller 1963; Tison *et al.* 1998). Because of the characteristic texture of congelation ice, it is also often referred to as columnar ice. In congelation ice, the structure of the ice-water interface is highly dependent on the purity of the source water and the growth velocity (Harrison and Tiller 1963; Lofgren and Weeks 1969; Wettlaufer 1992; Wettlaufer 1998). The microstructural morphology of the ice-ocean interface is related to the phenomenon of constitutional supercooling (Eicken 2003; Harrison and Tiller 1963), originally proposed and studied in the field of metallurgy (Jackson 2004; Rutter and Chalmers 1953). Constitutional supercooling refers to supercooling that occurs in advance of the freezing front. The role of constitutional supercooling in sea ice growth is critical to governing its substructure and in turn its properties (Eicken 2003; Petrich and Eicken 2017; Weeks 2010). Rejection of impurities locally enhances concentration and depresses the freezing point at the interface, promoting supercooling ahead of the interface. In the absence of this supercooled layer, small perturbations in the interface morphology are not energetically favorable and a planar interface is stable. If perturbations occur in the presence of constitutional supercooling, the supercooled fluid serves as a heat sink that promotes further growth, forming cells or dendrites. Characteristics of the interface (i.e. planar, cellular, dendritic) are significant to the efficiency of impurity incorporation in ice (Nagashima and Furukawa 1997). A relatively fresh source water is less prone to constitutional supercooling and is thus more efficient at rejecting impurities from the bulk ice due to a planar ice-water interface remaining stable (Eicken 2003). The opposite is true for saltwater, where a more textured ice-water interface, supported by constitutional supercooling, favors brine entrapment between cells (Eicken 2003; Osterkamp and Weber 1970; Petrich and Eicken 2017; Weeks 2010).

3.2. Examples of Frazil and Congelation Ice on Earth

We have selected five types of natural accreted ice to discuss in this work: sea ice, platelet ice, marine ice, sub-ice-shelf congelation ice, and “lake ice” (Fig. 2). The first four types of accreted ice represent the bounds of a parameter space defined by genetic classification (frazil vs. congelation) and temperature gradient (low vs. high). The temperature gradient controls the rate at which ice forms, which influences properties of the ice such as salinity. The temperature gradient scales with ice thickness, where deeper ice typically forms at a lower temperature gradient. “Lake ice” represents congelation ice formed under conditions where a planar ice-water interface remains stable.

Sea ice is one of the most ubiquitous and most studied forms of accreted ice on Earth. The thickness of sea ice typically does not exceed a few meters and as such presents with temperature gradients on the order of ten degrees per meter (Buffo *et al.* 2020; Weeks and Ackley 1986). The growth of sea ice is typically initiated by the formation of a thin wind-generated frazil ice layer, followed by congelation growth driven by conduction of heat from the ice-ocean interface through the overlying ice to the surface (Weeks and Ackley 1986). Sea ice has a cellular substructure, supported by constitutional supercooling, where impurities rejected upon freezing collect within brines that form in the grooves between ice plates and along the grain boundaries between crystals (Lofgren and Weeks 1969; Moore *et al.* 1994). Brines incorporated within the ice serve as habitats for organisms, where nutrients are replenished through convection-driven exchange with the underlying ocean (Loose *et al.* 2011). The structure and properties of sea ice described here also applies to ice formed from brackish or saline lake water (Leppäranta 2015). Analyses of sea ice cores suggest congelation ice dominates Arctic sea ice production, where typically only the uppermost layer is composed of frazil, whereas frazil can contribute significantly to Antarctic sea ice, particularly in the Weddell Sea (Gow *et al.* 1987; Lange *et al.*

1989). To distinguish it from congelation sea ice, sea ice layers formed from the incorporation of buoyant frazil beneath extant sea ice are referred to as platelet ice (Eicken and Lange 1989; Hoppmann *et al.* 2020; Lange 1988).

Platelet ice has broadly been used to refer to ice consisting of disk-shaped platelets, although a recent work has advocated for a more formal terminology (Hoppmann *et al.* 2020). These platelets are frazil crystals which grew within a supercooled water column, either at depth or near the ice-ocean interface (McGuinness *et al.* 2009; Smith *et al.* 2012; Smith *et al.* 2001), and became sufficiently buoyant to overcome turbulent suspension (Robinson *et al.* 2019). The term has been applied to both incorporated and loose platelet layers found beneath sea ice (Dempsey *et al.* 2010; Jeffries *et al.* 1995), where the semi-consolidated platelet layer beneath sea ice is sometimes referred to as the sub-ice platelet layer (Hoppmann *et al.* 2020). Although marine ice is a more common term to apply to platelet layers beneath ice shelves (Hoppmann *et al.* 2020), the term platelet ice has been used to describe ice accreted beneath ice shelves (Souchez *et al.* 1991). Analysis of ice core thin sections suggests the incorporation of platelet ice likely occurs by interstitial congelation growth (Gow *et al.* 1998; Jeffries *et al.* 1993; Smith *et al.* 2012).

Marine ice is specific to frazil ice that collects and consolidates beneath ice shelves or within ice shelf rifts. Because the mean thicknesses of ice shelves approach hundreds of meters, the temperature gradient could approach tenths to hundredths of a degree per meter. Temperature measurements of the marine ice layer beneath Amery Ice Shelf are consistent with these estimates of temperature gradient (Craven *et al.* 2009). Furthermore, these measurements indicate that the temperature profile is near-isothermal for a large fraction of the marine ice layer, extending from the ice-ocean interface, and that the temperature gradient approaches zero (Craven *et al.* 2009). This hydraulically connected region can extend from tens of meters up to ~100 m from the base of the ice shelf (Craven *et al.* 2009). Marine ice is thought to be more ductile than meteoric ice (Holland *et al.* 2009; Jansen *et al.* 2013; Kulessa *et al.* 2014; McGrath *et al.* 2014), but it is still an open area of research whether this is an intrinsic material property or because it is warmer than the surrounding meteoric ice. The deformation experiments of Dierckx and Tison (2013) on isotropic samples of marine ice from Nansen Ice Shelf suggest that the enhanced ductility of marine ice can be attributed to elevated temperatures alone. However, preliminary results from recent deformation experiments on anisotropic marine ice samples from Amery Ice Shelf, suggest that marine ice is softer than the surrounding meteoric at the same temperature (Craw 2020). The latter study is likely more representative of marine ice which has experienced continuous deformation, typical of an ice shelf (Craw 2020). Because of its distinct rheology, marine ice accretion is thought to play an important role in stabilizing ice shelves against collapse through the infilling of regions of weakness (Holland *et al.* 2009; Khazendar *et al.* 2009; Kulessa *et al.* 2014). Fractures propagating in ice shelves have been observed to arrest when encountering features infilled with marine ice (McGrath *et al.* 2014). The accretion of marine ice within suture zones has been shown to channel shear deformation enabling decoupling of adjacent units of ice flowing at different velocities (Jansen *et al.* 2013). The unique behavior and properties of marine ice can be attributed to its mechanism of formation.

The formation of marine ice is generally thought to occur in two phases, defined by Tison *et al.* (2001) as (1) the frazil ice phase and (2) the consolidation phase. The frazil phase encompasses the formation and accumulation of frazil ice crystals beneath the ice shelf. These crystals preferentially form and collect where the ice draft thins rapidly—features such as inverted channels, rifts, or crevasses beneath the ice shelf (Khazendar and Jenkins 2003; Khazendar *et al.* 2001; Tison *et al.* 1993). The consolidation phase involves the buoyancy-driven compaction of accumulated frazil crystals. In this phase, crystals agglomerate and collect, forming a permeable layer. As more frazil accumulates, buoyant pressure builds up at the ice-water interface, compressing the layer and forcing out interstitial water, reducing the brine volume fraction. The bulk density of the ice-brine system is thus counter-intuitively reduced by compaction. At a certain stage in the consolidation phase, the ice becomes impermeable and any remaining brine is trapped in the ice as inclusions at triple-junctions and along grain boundaries (Moore *et al.* 1994). The final stage of consolidation involves the freezing of remaining interstitial water through congelation growth, analogous to the incorporation of platelet ice layers beneath growing sea ice. Unlike platelet ice, this interstitial congelation growth occurs at a much slower rate due to the insulation from atmospheric thermal forcing by overlying glacial ice. The formation of marine ice beneath ice shelves is part of a process that has been referred to as an "ice pump", where the pressure dependence of the freezing point supports the operation of a continuous cycle involving the melting of ice at depth and the accretion of ice at a more shallow location (Lewis and Perkin 1986). The term marine ice is sometimes broadly applied to ice that forms beneath ice shelves. Here, however, we distinguish between marine ice and sub-ice-shelf congelation ice to emphasize the distinct formation mechanisms between these forms of accreted ice.

Because the ice-ocean interface beneath ice shelves is fairly insulated from atmospheric forcing (i.e., the ocean is shielded from frigid air temperatures by hundreds of meters of ice), the formation of congelation ice at the base of an ice shelf is rare (Fig. 4); however, it has been observed beneath certain ice shelves in Antarctica (Gow and Epstein 1972; Souchez *et al.* 1991; Zotikov *et al.* 1980). A simple model to predict the formation of congelation ice beneath an ice shelf was proposed by the Ross Ice Shelf Project (RISP) and summarized by Neal (1979). When water at the pressure-melting temperature flows in the direction of increasing ice shelf thickness, it must dissipate heat to remain at the pressure-melting temperature. Under conditions where the thickness gradient and flow speed are such that the sensible heat conduction to the overlying ice layer exceeds that which must be dissipated at the boundary layer to maintain the pressure-melting temperature, bottom freezing will occur (Neal 1979). The J-9 Ross Ice Shelf core represents a unique and valuable sample of congelation ice acquired at a depth of ~400 m within a zone of bottom freezing (Zotikov *et al.* 1980). The published sample is uniquely well-characterized for sub-ice-shelf congelation ice and includes measurements of salinity, grain size, texture, and freezing rate. The freezing rate estimate was obtained from an observed transition in growth conditions at the bottom 2 cm, which was attributed to localized melting caused by a drilling expedition the prior year (Zotikov *et al.* 1980). The estimate was validated by a simple heat transfer calculation (Zotikov *et al.* 1980) and represents the only estimate of sub-ice-shelf congelation ice growth rate obtained through direct inspection of a sample of the basal accreted ice. Congelation ice can also form beneath ice shelves experiencing high rates of surface ablation (e.g., locations with strong katabatic winds) (Souchez *et al.* 1991).

Lake ice is congelation ice that forms in an environment where constitutional supercooling is minimal (salinity $\lesssim$ 1–2 ppt), allowing a planar ice-water interface to remain stable (Grothe *et al.* 2014; Leppäranta 2015; Palosuo 1961; Weeks and Lofgren 1967). The clear glass-like texture characteristic of lake ice is a consequence of the stability of the planar interface, whereas ice with a cellular interface appears cloudy (Maus 2006; Petrich and Eicken 2017; Weeks and Lofgren 1967). Lake ice is a poor habitat relative to sea ice (Leppäranta 2015) since the planar ice-water interface is not conducive to the formation of permeable networks favorable to supporting in-ice habitats (Loose *et al.* 2011). However, where melt is generated within the ice layer and a supply of nutrients is accessible, lake ice can serve as a habitat in an otherwise unfavorable environment (Priscu *et al.* 1998).

These five examples of terrestrial accreted ice demonstrate that the environment in which the ice forms ultimately governs certain defining characteristics. Of these characteristics, salinity represents a critical state variable that (in addition to temperature) governs the distribution of stable brine (Cox and Weeks 1983). Brine volume fraction in turn determines the bulk thermophysical, dielectric, and mechanical properties of the ice (Thomas 2017). The implications of the distinct characteristics of accreted ice, in particular salinity, are important to consider when evaluating the habitability of icy ocean worlds.

4. **Salinity of Accreted Ice from Experiments and Ice Cores**

As ice forms, salts are rejected from the crystal lattice to the grain boundaries as brine. Select impurities, specifically chloride, fluoride, ammonium, and acids (H+), are soluble within the ice lattice and are accommodated as defects within the ice crystal. The total concentration of salts in ice, including both those accommodated within the lattice and those along grain boundaries, is referred to as the bulk salinity (Hunke *et al.* 2011). The efficiency of salt entrapment in ice is correlated to the ice growth velocity, which is directly proportional to the local temperature gradient at the freezing front (Buffo *et al.* 2020).

4.1. Congelation Ice across Growth Regimes

Historically, the salinity of sea ice was estimated using a theory adapted from the field of metallurgy, referred to as the Burton, Prim, and Slichter (BPS) model (Burton *et al.* 1953; Weeks and Lofgren 1967). In this model the partitioning of salt into ice, S_{ice}, from ocean water of salinity, S_0, is captured by the effective solute distribution coefficient, $k(v) = S_{ice}/S_0$, which is a function of ice growth velocity. Although the BPS model is only strictly valid for solute entrapment within the ice lattice, and not within interstitial brine pockets as is typical of sea ice (Weeks and Ackley 1986), the model fits the data well for both natural and artificial ice over a range of freezing rates (Fig. 3). Other authors have speculated that the success of the BPS model can be attributed to the number of free parameters (Notz and Worster 2009) and the insensitivity at high growth rates (Makkonen 1987). Contemporary work models sea ice as a mushy layer (Feltham *et al.* 2006), which has been demonstrated to reproduce salinity profiles in ice cores (Buffo *et al.* 2018; Griewank and Notz 2013; Wells *et al.* 2019). Mushy layer models demonstrate that the rejection of salts during the formation of ice can be attributed entirely to gravity drainage, a convection-driven desalination mechanism, and not segregation at an ice-ocean interface as represented by the BPS model (Notz and Worster 2009). Still, parameterizations of salt partitioning based on growth velocity could represent a computationally inexpensive approach to augment simple freezing models that do not directly model ice desalination processes.

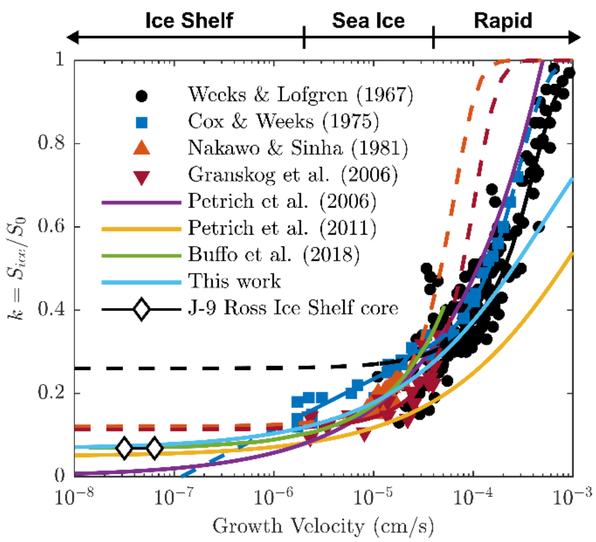

FIG. 3. Summary of relationships representing the effective solute distribution coefficient, $k = S_{ice}/S_0$, as a function of ice growth velocity. The markers represent data points from experimental or field data. Solid lines through data points represent fits of the data to the Burton, Prim, and Slichter (BPS) model (Burton *et al.* 1953; Weeks and Lofgren 1967), where dashed lines represent extensions of the model beyond the available data range. The experimental data of Weeks and Lofgren (1967), the field data of Nakawo and Sinha (1981), and the field data of Granskog *et al.* (2006) were digitized from published plots. The purple curve is a power law fit through the data of Nakawo and Sinha (1981), inspired by the form of the sea ice desalination model of Cox and Weeks (1988). The green curve is a smoothed representation of multiple runs of the mushy-layer model of Buffo *et al.* (2018).The yellow curve represents the model of Petrich *et al.* (2011), where $\gamma_s w_0 = 4.5 \times 10^{-8}$ m/s and $\phi_c = 0.05$. The light blue curve first presented here, represents a fit of the model of Petrich *et al.* (2011) to the data of Nakawo and Sinha (1981), yielding $\gamma_s w_0 = 3 \times 10^{-8}$ m/s, which is in-family with the value used by (Petrich *et al.* 2011). Both the smoothed model runs of Buffo *et al.* (2018) and our new fit of the model of Petrich *et al.* (2011) assume a critical porosity equal to the equilibrium distribution coefficient derived from the Ross Ice Shelf J-9 core, estimated by Buffo *et al.* (2020) to be $k_{eq} = 2.32/34$.

At growth velocities above those naturally occurring on Earth (Fig. 4), ice experiences minimal fractionation ($k \approx 1$) upon freezing, implying that it serves as a relatively unaltered chemical fingerprint of the source water. Published measurements of sea ice growth rates span from 0.15 cm/day (Souchez *et al.* 1988) to 3 cm/day (Shokr and Sinha 2015) or approximately 2×10^{-6} to 4×10^{-5} cm/s. Salt partitioning in this regime has been characterized using both natural (Granskog *et al.* 2006; Nakawo and Sinha 1981) and artificial (Cox and Weeks 1975; Weeks and Lofgren 1967) samples of congelation ice. The artificial samples correspond to ice formed through the freezing of sodium chloride solutions, ranging in salinity from 1 to 100 ppt. Studies of natural sea ice samples are more challenging due the difficulties in obtaining samples and the uncertainties in natural growth rates. The dataset of Nakawo and Sinha (1981) is particularly valuable because of the high sampling frequency of ice salinity and temperature they obtained over the growth season that produced nearly continuous profiles of ice salinity and growth rate.

At a certain stage in growth, the salinity profile of the ice no longer evolves in time due to progressive brine drainage. This salinity has been referred to as the stable salinity (Nakawo and Sinha 1981; Petrich *et al.* 2006) or steady-state salinity (Petrich *et al.* 2011). The natural congelation ice samples of Nakawo and Sinha (1981) in Fig. 3 are thought to be representative of this stable salinity and as such fall below the experimental data, which was not given sufficient time to reach this steady-state condition. The Baltic sea ice samples of Granskog *et al.* (2006) in Fig. 3 represent the stable salinity of ice formed from a lower salinity source water. These data suggest that a lower salinity source water may enhance the efficiency of salt rejection, possibly due to a change in interface morphology (Granskog *et al.* 2006). Their data are consistent with those of Weeks and Lofgren (1967), which included samples formed from low salinity source waters.

The model of Petrich *et al.* (2006) represents an empirical power law fit to the dataset of Nakawo and Sinha (1981), but underpredicts the distribution coefficient of the J-9 Ross Ice Shelf core (Zotikov *et al.* 1980), introduced in Section 3.2, and exceeds unity at high growth velocities. Their model also does not capture the physics of low porosity congelation ice, namely the existence of a percolation threshold which would limit salt expulsion from the growing ice. The model of Petrich *et al.* (2011) is a parameterization of the bulk salinity of sea ice as a function of growth velocity based on mushy-layer theory and represents steady-state conditions. Although the model has been validated through both fluid dynamics simulations and field data, it appears to underpredict the salinity of the Nakawo and Sinha (1981) samples. This could suggest that the stable salinity estimates of Nakawo and Sinha (1981) are too high, possibly biased by higher salinity values earlier in the growth season or that the ice may not have achieved a true steady-state by the end of the growth season. Their Fig. 8 seems to suggest the stable salinity may still be decreasing near the end of the growth season, although this could also signify the onset of the melt season since the gradual decrease in salinity becomes more pronounced around April.

Bulk salinity predictions which implement both mushy-layer theory and a critical porosity (Buffo *et al.* 2018; Petrich *et al.* 2011) best represent the physics of congelation ice desalination as it is understood today and as such serve as a strong foundation to obtain a parameterization of congelation ice salinity based upon growth velocity. Although these models deviate from each other above growth velocities of 10^{-5} cm/s, the model of Petrich *et al.* (2011) appears to represent a conservative lower bound. Furthermore, this model is well behaved across all growth regimes, such that k approaches unity for high growth velocities and $k = \frac{\rho_0}{\rho_i}\phi_c$ as the growth velocity approaches zero, analogous to the asymptotic salinity derived by Buffo *et al.* (2020). Note that this implies a lower bound distribution coefficient related to the critical porosity of the ice. We refer to this lower bound distribution coefficient, approached as the growth velocity decreases to zero, as the effective equilibrium solute distribution coefficient, k_{eq}.

4.2. Low Temperature Gradient Accreted Ice

For ocean worlds, we are interested in the accretion of ice in low temperature gradient environments characterized by growth velocities within the ice shelf regime ($< 10^{-6}$ cm/s), where $k \approx k_{eq}$ (Fig. 3). Because experimental studies cannot sample this growth velocity regime, we must leverage Earth's natural laboratory to constrain the salinity of ice formed in these environments. We present a survey of the available published ice core data from Antarctica, including samples of marine ice and sub-ice-shelf congelation ice (Fig. 4). We provide characteristics of the environment in which the ice formed, including depth from the surface as a proxy for temperature gradient (i.e., deeper ice implying a lower temperature gradient) and estimates of growth velocity where available. We also include properties of the ice such as salinity and $\delta^{18}O$, which can serve as a proxy for modification by glacial meltwater (i.e., values close to 2‰ implying minimal modification). $\delta^{18}O$ is often used to determine the origin of the ice (i.e., marine or meteoric) when the salinity signal is ambiguous (Gow and Epstein 1972; Morgan 1972; Oerter *et al.* 1992). Table 2 presents the values of k_{eq} estimated from selected ice cores in Fig. 4. We discuss how these values are obtained in the following sections.

Location	Site Description	Name	Type	Depth from Surface (m)	Salinity (ppt)	$\delta^{18}O$ (ppt)	k	Growth Velocity (cm/s)	Source(s)
Amery Ice Shelf	Suture Zones	G1	M	270 – 315	0.05 – 0.1	0 – 2	10^{-3}	1×10^{-6}	Morgan (1972)
		AM01	M	276 –376	0.03 – 0.56	2	10^{-4} –10^{-3}	3×10^{-6}	Craven et al. (2004, 2009)
Roi Baudouin Ice Shelf	Rift Exposed at Surface	D	M	10 – 20	0.3 – 9	2	10^{-2} – 10^{-1}	-	Pattyn et al. (2012)
		E	M	0 – 15	0.3 – 2	2	10^{-3} – 10^{-2}		
Filchner-Ronne Ice Shelf	Thin Region beyond Henry Ice Rise	B13	M	152.8 – 215	0.02 – 0.1	2	10^{-4} – 10^{-3}	4×10^{-6}	Oerter et al. (1992) Eicken et al. (1994)
Ross Ice Shelf	Region of Heat Loss to the Ice Shelf	J-9	SISC	410 – 416	2 – 4	-	10^{-3} – 10^{-2}	6×10^{-8}	Zotikov et al. (1980)
McMurdo Ice Shelf	Exposed at Surface near Minna Bluff	Site 3	M	0 – 5	0.115	2.3	10^{-3}	-	Fitzsimons et al. (2012)
		C5	M	0 – 2.65	0.26 ± 0.11	1.63 ± 0.24	10^{-3}	-	Koch et al. (2015)
		C9	M	0 – 3.04	0.20 ± 0.15	1.64 ± 0.43	10^{-3}		
		C15	M	0 – 9.44	0.29 ± 0.18	0.47 ± 0.48	10^{-3}		
Dailey Islands	Exposed at Ice Shelf Surface	No. 1	M	0 – 6.74	0.01 – 0.09	-	10^{-4} – 10^{-3}	-	Gow et al. (1965)
		No. 2	M	0 – 15.25	0.01 – 0.05	-	10^{-4} – 10^{-3}		
Koettlitz Glacier Tongue	Exposed at Surface of Glacier Tongue	1	SISC	0 – 12.8	0.2 – 3.76	2.51 – 1.61	10^{-3} – 10^{-1}	-	Gow and Epstein (1972)
		3		0 – 13	2.19 – 5.26	1.76 – 1.85	10^{-2} – 10^{-1}		
Nansen Ice Shelf	Exposed in Rift at Ice Shelf Surface	NIS	M	0 – 45	0.005 – 0.19	1.80 – 2.37	10^{-4} – 10^{-3}	2×10^{-6}	Khazendar et al. (2001) Tison et al. (2001) Khazendar et al. (2003)
Hells Gate Ice Shelf	Exposed at Ice Shelf Surface	Granular	M	0 – 1.5	0.016 – 0.081	2 – 3.5	10^{-4} – 10^{-3}	3×10^{-7}	Souchez et al. (1991)
		Columnar	SISC	0 – 1.5	1.6 – 2.6	1 – 2	10^{-2}		
		Platelet	M	0 – 1.5	0.24 – 0.49	2 – 3.5	10^{-3} – 10^{-2}		
Arctic	"Ice Island"	SP-6	SISC	0 – 9	0 – 3	-	10^{-2}	-	Cherepanov (1964)
	Sea Ice	9a	CS	0 – 1.5	4 – 7.5	-	10^{-1}	1×10^{-5}	Nakawo and Sinha (1981)

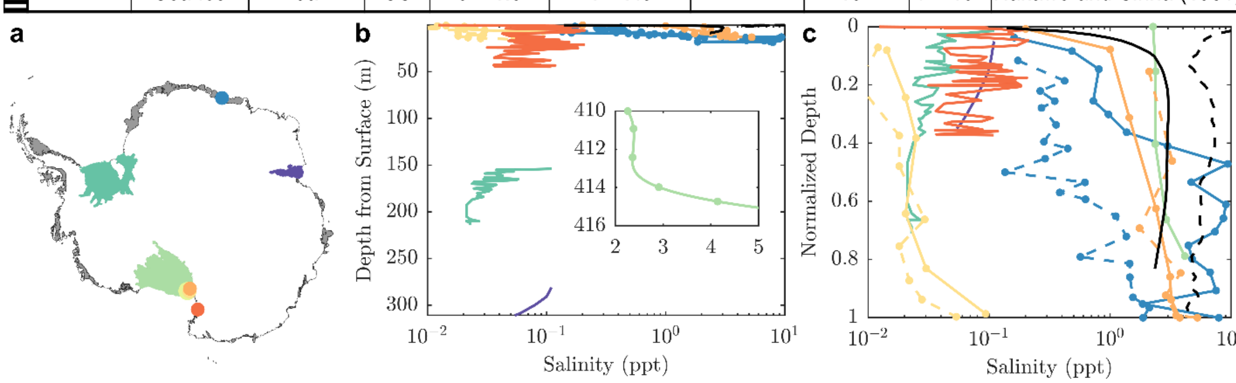

FIG. 4. A summary of properties and characteristics of terrestrial accreted ice from published ice core data. The first two columns specify the location where the ice core was collected and a description of the sample site. The sites are color and texture coded by ice shelf and presented in the map of Antarctica in **(a)**. Where multiple cores were collected from a single location, the second core is represented as dashed. The third column provides the name of the ice core or ice type as referenced in the sources in the rightmost column. The type of accreted ice is specified in the fourth column according to the following codes: M (Marine Ice), SISC (Sub-Ice-Shelf Congelation Ice), CS (Congelation Sea Ice). The depth associated with the ice core samples is presented in the fifth column and inversely correlates to the temperature gradient (i.e., deeper ice implies a lower temperature gradient). The salinity references either the published ice core salinity values, where available, or the practical salinity estimated from the published conductivity measurements, assuming a temperature of 20 °C (Lewis and Perkin 1981). Where a single value is provided to represent salinity instead of a range, this value corresponds to the mean. Note that salinities of the Hells Gate Ice Shelf samples were scaled from sodium content, assuming total salt content is 30.74% sodium (Souchez *et al.* 1991). The $\delta^{18}O$ reflects the published values obtained from the ice core samples and represents a proxy for the modification of ocean water by glacial meltwater, where values below 2‰ could suggest some modification. The effective distribution coefficients provided in the table were obtained by dividing the ice salinity by 35 ppt. Growth velocity estimates were included when provided in the published works. The plots representing the **(b)** absolute and **(c)** depth-normalized salinity profiles follow the same color and texture coding represented in the table and map. The plots represent data digitized from the published works referenced in the rightmost column. Markers in the profiles represent digitized datapoints whereas curves reflect the digitized representation of profiles.

4.2.1. Sub-Ice-Shelf Congelation Ice

Because salt is predominantly trapped within pore spaces as brine in congelation ice, the steady-state salinity is thought to be coupled to a critical porosity (~5%) below which ice is thought to be impermeable to brine transport (Golden *et al.* 1998; Golden *et al.* 2007). The critical porosity is typically a prescribed parameter in numerical models of sea ice salinity (Buffo *et al.* 2018; Griewank and Notz 2013; Petrich *et al.* 2011; Wells *et al.* 2019) and governs the finite ice salinity that the model asymptotically approaches as the growth velocity approaches zero and the system reaches equilibrium (Fig. 3). The distribution coefficient associated with this limit has been referred to as the equilibrium distribution coefficient (Burton *et al.* 1953; Weeks and Lofgren 1967) and would represent the bulk salinity of congelation ice as the growth velocity approaches zero.

Samples of congelation ice formed in low temperature gradient environments are limited (Fig. 4). Unlike sea ice, where growth velocities can be estimated by periodic measurements over the growth season (Nakawo and Sinha 1981), estimates of growth velocity for congelation ice beneath ice shelves are obtained using models. Certain ice cores collected from ice shelves in Antarctica (Ross Ice Shelf, Koettlitz Glacier Tongue, Hells Gate Ice Shelf) were observed to have the columnar texture indicative of congelation ice (Gow and Epstein 1972; Souchez *et al.* 1991; Zotikov *et al.* 1980). Published estimates of the growth velocities associated with accreted ice found beneath ice shelves (Fig. 4) are well within the asymptotic growth velocity regime of the models in Fig. 3. Because of its extensive thickness, the sea ice island SP-6 likely approaches temperature gradients within this regime and is thus classified as sub-ice-shelf congelation ice (Fig. 4). The salinity of accreted ice at these low temperature gradients can thus be used to constrain k_{eq} for congelation ice (Table 2).

The bottom 2 cm of the Ross Ice Shelf core was described to have a “waffle-like” texture, consistent with an actively growing congelation ice layer with an unstable interface (Zotikov *et al.* 1980), often referred to as a “skeletal layer” (Buffo *et al.* 2020). The salinity profile reveals a transition at approximately 2 m above the ice-ocean interface from constant to monotonically increasing with depth (Fig. 4b). In sea ice, an increase in salinity with depth near the base is recognized to be a feature of growing sea ice (Eicken 1992). The increasing salinity observed near the base of the Ross Ice Shelf core and the description of the basal texture suggest the bottom 2 m of the Ross Ice Shelf core is in a state of active desalination. However, the constant salinity observed above this transition can be considered the stable salinity, attained at growth rates within the asymptotic regime (Fig. 3, 4), and can thus be used to obtain an estimate of k_{eq} (Table 2). The salinity profiles associated with the Koettlitz Glacier Tongue ice cores do not appear to have achieved a stable salinity, particularly the ice sampled from Hole 3 (Fig. 4c). This interpretation is supported by samples of seawater obtained from the bottom of Hole 3, which was found to be enriched in salt, suggesting the ice in this location is also actively desalinating (Gow and Epstein 1972). Additionally, the $\delta^{18}O$ signal shows slight modification of the ice source water by glacial meltwater. These observations suggest that the Koettlitz Glacier Tongue ice cores may not be representative of an equilibrium state of salt partitioning, although the salinity profile of Hole 1 suggests a stable salinity could fall between 2 and 3 ppt which is in-family with the Ross Ice Shelf core. A salinity profile is not available for the Hells Gate Ice Shelf columnar ice (Souchez *et al.* 1991); however, the $\delta^{18}O$ signal presents with some evidence of modification by glacial meltwater. Therefore, we adopt the maximum observed salinity to estimate a value for k_{eq}. The salinity profile associated with Ice Island SP-6 drops off sharply near the ice-atmosphere interface (Fig. 4c) which is indicative of post-genetic brine redistribution (Eicken 1992). As such, for SP-6, we adopt the salinity at the base and the mean salinity to estimate bounds on k_{eq}. The equilibrium distribution coefficients derived from these congelation cores are in family with one another and on the order of 10^{-2} (Table 2). Of the sub-ice-shelf congelation cores considered here, the salinity profile associated with the Ross Ice Shelf core shows the least evidence of post-genetic desalination or brine redistribution. The stable salinity of this ice core is representative of the equilibrium distribution coefficient for natural congelation ice, $k_{eq} = 6.7 \times 10^{-2}$, which is the same value inferred for the upper bound of the SP-6 core (Table 2). Notably, this value is similar to the critical porosity of 5% discussed in the previous section, lending credence to its role in governing the stable salinity of congelation ice.

4.2.2. Marine Ice

The distribution coefficients associated with marine ice can be lower than the equilibrium distribution coefficients for congelation ice by up to an order of magnitude (Table 2 and Fig. 4), generally falling between 10^{-4} and 10^{-3} (bulk salinities between 10^{-2} and 10^{-1} ppt). The salinity profiles associated with marine ice (Fig. 4b,c) generally appear to depict a decrease with distance from the meteoric-marine interface within the impermeable portion of the ice core and an increase from the permeable-impermeable boundary to the ice-ocean interface. Note that many of the profiles depicted in Fig. 4 do not extend to the permeable layer, so we must rely on descriptions of the drilling and isolated samples reported in the published works to infer its properties.

The salinity profiles of the Roi Baudouin Ice Shelf cores are anomalously high relative to those of other marine ice cores (Fig. 4b,c) and approach values comparable to that of sea ice. Recent consolidation was proposed as an explanation for the high salinity of the Roi Baudouin cores (Pattyn *et al.* 2012), implying that young marine ice may initially present with salinities commensurate with sea ice but will gradually desalinate and approach a steady state over time due to increased accumulation and consolidation. This interpretation is supported by their salinity profiles, which depict a stable salinity similar to that of the marine ice at McMurdo Ice Shelf that transitions to an increasing salinity with depth (Fig. 4c). The discovery of tubular conduits in the relatively unconsolidated marine ice section of the Roi Baudouin Ice Shelf cores support the interpretation of a young marine ice in the early stages of consolidation where desalination processes are still actively occurring (Hubbard *et al.* 2012). These conduits were observed to have a structure different from the brine drainage channels found in congelation sea ice, specifically lacking a vertical "tree-like" structure (Hubbard *et al.* 2012). An alternative explanation is that the Roi Baudouin marine ice formed in a high temperature gradient environment and is analogous to platelet ice. However, the site is not unlike the rift at Nansen Ice Shelf where the salinity of the marine ice there was found to be in-family with other marine samples (Khazendar *et al.* 2001; Tison *et al.* 2001). The rift at Nansen Ice Shelf is located in an area with strong katabatic winds, which could result in the ablation of the marine ice which originally infilled the rift (Khazendar *et al.* 2001). This suggests the marine ice exposed at the surface may have formed at a lower depth, much like at Hells Gate Ice Shelf where katabatic winds expose basal marine ice at the surface near the ice shelf terminus (Souchez *et al.* 1991). This suggests marine ice at Nansen ice shelf may have initially shared characteristics with that of Roi Baudouin but became more homogenous and consolidated over time.

The age of the marine ice appears to be a more dominant factor in governing the bulk salinity than the temperature gradient, supporting the idea that the consolidation mechanism is a compaction and not congelation process. This is evident from the plots in Fig. 4c which demonstrate that increased depth does not correlate to decreased salinity. The salinities of the Nansen Ice Shelf core, Filchner-Ronne Ice Shelf core, and the Amery Ice Shelf core are approximately equal although they were sampled from depths that differed by over 100 m from each other. The profiles associated with the Amery Ice Shelf and Nansen Ice Shelf cores suggest the salinity could continue decreasing beyond the region sampled. The Filchner-Ronne Ice Shelf core, on the other hand, shows evidence of achieving a stable salinity near the base of the core. The Dailey Island cores obtained within 10 m of the surface have salinities even lower than the preceding cores (Fig. 4c); although because $\delta^{18}O$ was not measured, the role of glacial meltwater in reducing the salinity cannot be discounted. We thus adopt $k_{eq} = 6.9 \times 10^{-4}$ for marine ice, which corresponds to the stable salinity of the consolidated layer estimated using the salinity at the base of the Filchner-Ronne Ice Shelf core (Fig. 4).

TABLE 2. Equilibrium distribution coefficients inferred from published samples of natural accreted ice from Earth. Values were derived using the minimum salinity observed in the core and an ocean salinity of 35 ppt. Where a trend (either increasing or decreasing) was absent in the salinity profile, the mean salinity was adopted instead. Only ice cores where melt water did not appear to contribute significantly to the salinity signal (i.e. $\delta^{18}O \approx 2$ in Fig. 4) were included. Ice type follows the same coding presented in Fig. 4 (SISC: Sub-Ice-Shelf Congelation Ice, M: Marine Ice).

k_{eq}	Ice Type	Sample	Source
6.71E-02	SISC	J-9 Ross Ice Shelf core	(Zotikov *et al.* 1980)
6.46E-02 – 6.71E-02	SISC	Ice Island SP-6 core	(Cherepanov 1964)
6.29E-02	SISC	Ice Island SP-4 core	(Cherepanov 1964)
1.43E-03	M	AM01 Amery Ice Shelf core	(Morgan 1972)
6.86E-04	M	B13 Filchner-Ronne Ice Shelf core	(Moore *et al.* 1994)
5.71E-03	M	C9 McMurdo Ice Shelf core	(Koch *et al.* 2015)
1.71E-03	M	Nansen Ice Shelf core	(Tison *et al.* 2001)
4.57E-04	M	Granular ice from Hells Gate Ice Shelf	(Souchez *et al.* 1991)

5. **Accretion beneath the Ice Shells of Ocean Worlds**

Although there have been no direct observations of the interior of the ice shells of ocean worlds, features observed at the surfaces have led to the development of hypotheses for processes that either directly appeal to the accretion of ice at the ice-ocean interface or are consistent with conditions that promote it (Běhounková *et al.* 2017; Buffo *et al.* 2020; Čadek *et al.* 2019; Howell and Pappalardo 2018; Manga and Michaut 2017; Michaut and Manga 2014; Soderlund *et al.* 2020; Soderlund *et al.* 2013). These surface features are scars of processes which modify bulk ice shell properties and serve as a record of heterogeneities introduced into the native shell.

5.1. Congelation Ice Shell

We model the native ice shell as the product of congelation ice growth at the ice-ocean interface driven by cooling of the interior. A simple 1D freezing model, represented by the Neumann solution to the Stefan problem with a temperature boundary condition, allows us to estimate ice shell growth rate (Fig. 5). We assume the ocean is at the melting temperature of 270 K and that the thermophysical properties of the ice shell are represented by pure ice at this same temperature. We evaluate four cases, assuming a boundary condition of 50 K, 100 K, 200 K, and 250 K to approximate surface temperatures expected at icy ocean worlds. 50 K represents a lower bound surface temperature for both Europa and Enceladus, 100 K represents the mean annual surface temperature of Europa's ice shell (Ashkenazy 2019; Ojakangas and Stevenson 1989), 200 K represents the maximum temperature near the tiger stripes of Enceladus (Spencer *et al.* 2018), and 250 K is intended to represent a terrestrial boundary condition. Higher surface temperatures result in lower growth rates for a given ice shell thickness. Using this model, we can estimate an upper bound on ice shell growth rate and thus constrain the maximum salinity of the bulk ice shell.

Instead of explicitly modeling salt rejection, like Buffo *et al.* (2020), we represent the incorporation of salt as a function of growth velocity using a model for $k(v)$, adapted from Petrich *et al.* (2011). This model assumes a cellular ice-water interface is maintained for all growth velocities and as such would not be applicable to dilute solutions. We prescribe a critical porosity equal to the effective equilibrium distribution coefficient for congelation ice $\phi_c = k_{eq}$, as opposed to $\phi_c = 0.05$ which is used in the model of Petrich *et al.* (2011), and force the model to approach this value at low growth velocities. This yields an expression for the effective solute distribution coefficient given by

$$k(v) = k_{eq}\left(1 + \frac{k_{eq}}{2}\frac{v}{\gamma_s w_0}\left[-1 + \sqrt{1 + \frac{4(1-k_{eq})}{{k_{eq}}^2}\frac{\gamma_s w_0}{v}}\right]\right) \tag{1}$$

where k_{eq} represents the effective equilibrium solute distribution coefficient for congelation ice, v is the ice growth velocity, and $\gamma_s w_0$ represents a scaling parameter related to the interstitial brine velocity (Petrich and Eicken 2017). Note that our version includes an additional factor of 2 that was excluded from a term in the radicand in the published versions of the original model (Petrich and Eicken 2017; Petrich *et al.* 2011). We find that the growth velocity transitions to the ice shelf regime (Fig. 3) below ~100 m depth for all surface temperatures considered. This is in-family with the results of Buffo *et al.* (2020) which found the salinity profile approaches an asymptotic value below ~300 m. This implies that the bulk salinity for a large fraction of the ice shell will correspond to a value approaching the equilibrium distribution coefficient. Note that the lower limit bulk ice shell salinity predicted by Buffo *et al.* (2020) corresponds to an equilibrium distribution coefficient governed by the apparent critical porosity in congelation ice (~0.05). This is similar to the magnitude of effective equilibrium distribution coefficients estimated from the congelation ice cores in Table 2.

Although the critical porosity appears to be a significant factor governing the equilibrium distribution coefficient in congelation ice, as the growth velocity approaches zero, the ice-water interface geometry should become planar and as a result will be incapable of entrapping brine (Eicken 1998), forming "lake ice". The development of a stable planar interface under the appropriate growth conditions is a phenomenon that has been studied in both nature and laboratory experiments for decades (Grothe *et al.* 2014; Weeks and Lofgren 1967). In experiments the transition from a cellular to planar interface coincides with a drastic change in appearance (cloudy to clear) and a reduction in distribution coefficient that can exceed an order of magnitude (Kvajić and Brajović 1971; Maus 2006; Osterkamp and Weber 1970; Weeks and Lofgren 1967). This suggests a critical growth velocity exists at which the mode of salt entrapment becomes independent of critical porosity.

The magnitude of the critical growth velocity is challenging to constrain. Morphological stability theory (MST), originally proposed by Mullins and Sekerka (1964), has been leveraged by a number of authors to investigate the development of a cellular interface in the freezing of saltwater systems (Maus 2007; Wettlaufer 1992). The theory has been augmented through the years (Coriell *et al.* 1985; Sekerka *et al.* 2015) and is still an active area of research (Maus 2020).

The theory predicts the existence of a critical growth velocity below which a planar ice-water interface should be stable for any wavelength perturbation. The magnitude of this critical growth velocity is poorly constrained by theory and is highly sensitive to parameters including the solution concentration, the distribution coefficient, and the temperature gradient in the liquid (Maus 2006; Maus 2020; Terwilliger and Dizio 1970; Wettlaufer 1992). To illustrate the onset of this transition during the thickening of an ice shell (Fig. 5), we adopt the value obtained by Wettlaufer (1992) from a linear stability analysis of the interface morphology of a sodium chloride system for a solution concentration approximately equal to Earth's ocean (~35 ppt). The critical growth velocity of $v_c \approx 10^{-8}$ cm/s is reached at an ice shell thickness of ~20 km for all surface temperatures considered (Fig. 5). Again, note that the magnitude of the critical velocity is poorly constrained, and we adopt the value in Fig. 5 for illustration purposes only. For example, Wettlaufer (1992) showed the critical velocity decreased to $v_c \approx 10^{-10}$ cm/s when assuming a distribution coefficient of 0.003 instead of 0.3. Their results demonstrate that the more efficient the ice is at rejecting the solute, the lower the critical velocity for the onset of interface instability for a given solution concentration. They also showed that reducing the solution concentration increases the critical velocity, explaining why a planar ice-water interface is stable for terrestrial lake ice growth conditions.

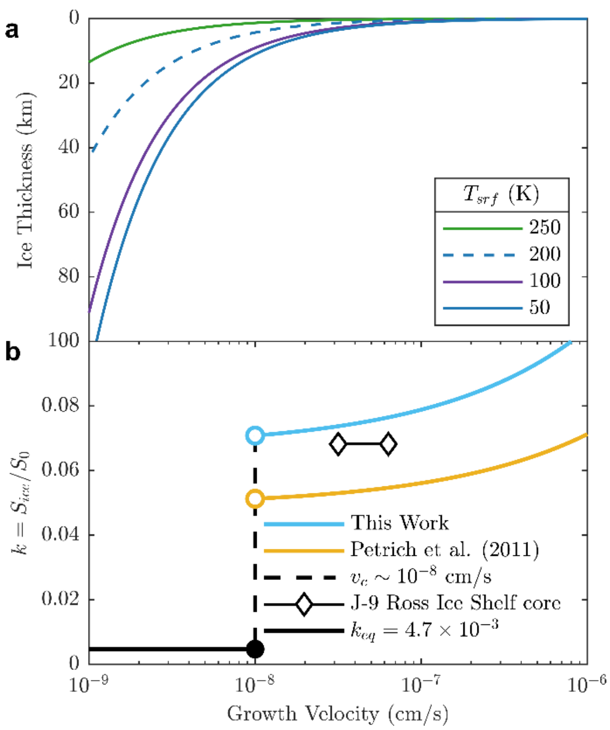

FIG. 5. (a) Ice shell thickness and **(b)** effective solute distribution coefficient as a function of growth velocity. Ice shell thickness and growth rate are modeled using the 1D Neumann solution to the Stefan problem for a range of surface temperature boundary conditions. The thermophysical parameters of the ice shell are assumed to be at a melting temperature of 270 K. The solute distribution coefficient curves are obtained from the model of Petrich *et al.* (2011), where the blue curve represents an adaptation of the model presented in this work and the yellow represents the original published model (also shown in Fig. 3). The dashed line represents an illustration of the transition from a cellular interface to a planar interface at a critical growth velocity, v_c. The assumed critical growth velocity is on the order of that found by Wettlaufer (1992) for parameters assumed to represent freezing of a terrestrial ocean. The value of equilibrium distribution coefficient is assumed from Gross *et al.* (1977) for ice chlorinity greater than the lattice solubility limit, where some interstitial accommodation of impurities occurs. The diamond markers represent the bounds of growth velocity estimated by Zotikov *et al.* (1980) for the J-9 Ross Ice Shelf core.

Below the critical velocity, we assume a planar-ice water interface remains stable and that the bulk salinity of the ice shell will be governed by the equilibrium distribution coefficient for congelation “lake ice”, where impurities are retained predominantly within the ice lattice (i.e., not incorporated interstitially as brine). Soluble salts can be accommodated in the ice lattice only up to a certain concentration referred to as the solubility limit. From both natural and artificial samples, the solubility limit for chloride in ice has been inferred to be $\sim 300\ \mu$M (Gross *et al.* 1977; Moore *et al.* 1994; Seidensticker 1972), although in the presence of ammonium the solubility limit increases (Gross *et al.* 1977). There is some evidence that the solubility limit may be higher in ice that has undergone recrystallization (Moore *et al.* 1994), suggesting marine ice may be able to accommodate more chloride than sub-ice shelf congelation ice. The chloride distribution coefficients obtained by Gross *et al.* (1977) represent salt entrainment through incorporation of impurities in the ice lattice and serve as the lower bound of equilibrium distribution coefficients for congelation ice. Their values are in-family with earlier works that estimated equilibrium distribution coefficients on the order of 10^{-3} for dilute ($\sim 2 \times 10^{-4}$ M) chloride solutions (Osterkamp and Weber 1970). For solution concentrations where chloride could be entirely accommodated within the ice lattice ($\lesssim 10^{-1}$ M) and did not occupy interstitial sites, the average equilibrium distribution coefficient was determined to be $k_{eq} = 2.7 \times 10^{-3}$ (Gross *et al.* 1977). Note that this distribution coefficient applies to chloride and not the associated cation pair, which was found to be significantly less soluble (Gross *et al.* 1977). In the presence of ammonium, the equilibrium distribution coefficient increased to $k_{eq} = 1.4 \times 10^{-2}$ (Gross *et al.* 1977). For more concentrated solutions, the solubility limit was exceeded upon crystallization, forcing residual impurities to be accommodated interstitially along grain boundaries. In this case the distribution coefficient increased to $k_{eq} = 4.7 \times 10^{-3}$ (Gross *et al.* 1977; Tison *et al.* 2001). Although the distribution coefficient almost doubled at this transition, it was independent of the solution concentration both below and above this transition. It is unclear whether a solution composed entirely of insoluble salts, such as magnesium sulfate, would be accommodated as efficiently because it would be limited to interstitial sites. It is also possible that because of its inability to be accommodated in the lattice, a solution dominant in lattice insoluble salts may promote interface breakdown and enhance interstitial entrapment.

These models imply that the native bulk salinity of a congelation ice shell should be <10% of the ocean salinity, where sub-ice-shelf congelation ice cores imply a bulk salinity between 6% and 7%. If the ice shell thickening is sufficiently slow, such that a planar interface remains stable as the ice shell thickens, the ice shell salinity reduces to <1% of the ocean salinity. For a planar interface at near-equilibrium conditions, the salts entrained are dominantly lattice soluble salts, such as chloride. The experiments of Gross *et al.* (1977) suggests the ice chlorinity will be 0.27% of the ocean chlorinity. In the case that the chlorides cannot be entirely accommodated within the lattice, the ice shell chlorinity will be 0.47% of the ocean chlorinity and permit some interstitial incorporation of impurities. If interstitial impurities are preferentially removed due to flushing or drainage, the bulk salinity would be governed by concentration of impurities accommodated in the ice lattice. For ice saturated with chloride, this would imply an ice shell chlorinity of ~10 mg/kg which is on the order of ice shell salinity predicted by Steinbrügge *et al.* (2020). The order of magnitude differences in bulk salinity due to transitions in growth velocity regimes could generate vertical and regional heterogeneities in ice shell salinity.

5.2. Local and Regional Accretion of Frazil Ice

The ice-ocean interfaces of icy ocean worlds represent dynamic environments characterized by gradients in ice thickness on both regional and local scales (Čadek *et al.* 2019; Hemingway and Mittal 2019; Nimmo and Bills 2010; Nimmo *et al.* 2007; Soderlund *et al.* 2020; Soderlund *et al.* 2013).

Rifts and basal features, such as crevasses and troughs, represent favorable locations for the formation and accretion of frazil ice in an ice shell. A number of processes have been demonstrated to generate stresses sufficient to cause fracturing in the ice shell including impacts (Craft and Roberts ; Turtle and Pierazzo 2001), pressurization due to cooling and thickening (Hemingway *et al.* 2020; Johnston and Montési 2017; Manga and Wang 2007; Nimmo 2004b), tidal forcing/nonsynchronous rotation (Geissler *et al.* 1998; Greenberg *et al.* 1998; Helfenstein and Parmentier 1985; Hoppa 1999; Hurford *et al.* 2007; Lee *et al.* 2005; Patthoff *et al.* 2019;

Rhoden *et al.* 2012), and true polar wander (Rhoden *et al.* 2011; Schenk *et al.* 2008; Tajeddine *et al.* 2017).

The fracturing of an ice shell has important implications for surface-ice-ocean exchange and as such has been studied extensively. Early work by Crawford and Stevenson (1988) examined both surface and basal fractures as resurfacing mechanisms for Europa's ice shell. They found that direct conduits extending from the surface through an ice shell were unlikely due to the need for high stresses applied rapidly which cannot be supplied by any process thought to be operating at Europa. Basal fractures were also shown to be incapable of extending to the surface; however, they extended over an order of magnitude farther than surface fractures. Although basal ice is ductile, Crawford and Stevenson (1988) argue that crack initiation and propagation is possible if the ice is strained sufficiently rapidly compared to the Maxwell time. This condition is possibly satisfied by the eccentricity tides which are ~10^5 s and comparable to the Maxwell time of ~10^4 s (Crawford and Stevenson 1988). The model of Lee *et al.* (2005) showed that surface fractures could penetrate the entire brittle part of the ice shell, in the case where a brittle and ductile layer are mechanically decoupled. They did not study basal fractures, citing that they were less likely to occur than surface fractures based on the increase in ice strength with depth, due to pore closure, and their interpretation of the results of Crawford and Stevenson (1988). Rudolph and Manga (2009) show that in the presence of a relaxed basal layer, fractures on Europa cannot penetrate the ice shell for thicknesses greater than a few kilometers. Because the gravitational acceleration at Enceladus is a fraction of that at Europa, fractures could penetrate the ice shell for thicknesses up to tens of kilometers (Rudolph and Manga 2009). The ice shell thickness where the tiger stripes are located is thought to be less than 10 km (Hemingway *et al.* 2020), supporting the interpretation that these features are fractures connecting the ice shell surface to a subsurface ocean (Postberg *et al.* 2011; Spencer *et al.* 2018). The ice collapse model of Walker and Schmidt (2015) suggests basal fractures could form above a subsurface water pocket; however, this mechanism would not necessarily translate to the formation of basal fractures at an ice-ocean interface. Hemingway *et al.* (2020) argue that a surface fracture could penetrate a ductile ice layer in an ice shell, so long as it is not too thick, because the layer will behave elasticity on timescales relevant to fracture propagation.

Broadly these works suggest basal fractures extending into the ice shell interior are possible—if the basal ice is subject to a sufficiently high strain rate—and that rifts extending through the entirety of an ice shell are unlikely for Europa. Still, many authors who attribute surface features at Europa such as domes, pits, and lenticulae to the presence of sills within the ice shell implicate vertical fractures extending from the ice-ocean interface (Craft *et al.* 2016; Michaut and Manga 2014). Furthermore, observations and interpretations of putative plume activity at Europa (e.g., Jia *et al.* 2018; Sparks *et al.* 2017) and Enceladus (e.g., Postberg *et al.* 2011) provide strong evidence that fractures in the ice shell serve as a connection between the surface and some subsurface water reservoir. Where cracks may penetrate the entirety of an ice shell, such as the tiger stripes at Enceladus, the resulting plumes would likely include samples of relatively unfractionated ice formed from agglomerated frazil crystals that nucleated within the turbulent, supercooled water column as the ocean water was brought to the surface. Given the high rate of ice formation, the salinity and compositional signal likely experiences minimal fractionation, $k \approx 1$. If the plume material were sourced from a reservoir generated from the melt of native ice shell material and not the ocean, our estimate of the distribution coefficient for a congelation ice shell predicts a saturated ocean (20 ppt/0.067 ~ 300 ppt). This estimate neglects the effect of brine concentration that may occur during freezing of a reservoir.

Ice shell thickness variations on regional scales have been inferred from models and observations of ocean worlds. Models of the ice shell thickness of Enceladus based on observations of the shape (Tajeddine *et al.* 2017) and gravity (Iess *et al.* 2014) by *Cassini* suggest the presence of lateral variations in the ice shell thickness (Čadek *et al.* 2019). Limb profiles of Europa suggest either a thin ice shell (<35 km) with lateral thickness variations below the detection threshold or a thicker shell in which lateral flow or convection promote a uniform ice shell thickness (Nimmo *et al.* 2007). Although the ice shell thickness of Europa is more poorly constrained than Enceladus (Billings and Kattenhorn 2005), multiple models have demonstrated variations in surface temperature and basal heat flux could promote lateral thickness gradients (e.g., Ashkenazy *et al.* 2018; Čadek *et al.* 2019; Soderlund 2019; Soderlund *et al.* 2013). These lateral thickness gradients could plausibly occur in any icy ocean world with large surface temperature gradients in latitude and/or heterogeneous tidal heating. Because these lateral thickness gradients are unstable (both from a mechanical and thermodynamic perspective), mechanisms will operate to homogenize the ice shell thickness.

Two mechanisms have been proposed for the homogenization of ice shell thickness: (i) the pressure gradient induced by the variable ice thickness will drive basal ice flow from thicker to thinner regions of the ice shell (e.g., Ashkenazy *et al.* 2018; Nimmo 2004a; Nimmo *et al.* 2007; Ojakangas and Stevenson 1989) and (ii) an "ice pump", described by Lewis and Perkin (1986), will operate to melt ice where the ice shell is thick and accrete ice where the ice shell is thin (e.g., Soderlund *et al.* 2013; Vance and Goodman 2009). Both properties likely play a role in homogenizing ice shell thickness gradients, although environmental factors such as ocean circulation and tidal velocity will determine which process dominates (Goodman 2018). The ice flux resulting from viscous flow at the base of the ice shell has been estimated to range from fractions of a millimeter to centimeters per year (Ashkenazy *et al.* 2018), whereas marine ice accretion rates on Earth, driven by the "ice pump" are on the order of meters per year (Craven *et al.* 2009). We thus focus our discussion on the "ice pump" which could infill these features on shorter timescales than viscous flow. As the buoyant meltwater is transported along the ice-ocean interface in the direction of decreasing ice thickness, it will become supercooled due to the reduction in pressure and prime the generation of frazil ice.

For terrestrial ice shelves, the ice pump process is approximately adiabatic (Foldvik and Kvinge ; Hoppmann *et al.* 2020; Koch *et al.* 2015; Tison *et al.* 1998). Neglecting heat transfer between water masses is likely only a valid assumption over certain temporal and spatial scales, which may be exceeded when applied to regional scale thickness gradients in the ice shells of ocean worlds. Crevasses, troughs, and rifts, on the other hand, represent high gradient features that can promote substantial supercooling through the operation of a highly localized ice pump. The magnitude of potential supercooling will be governed by the feature's vertical extent in the ice shell, equivalent to the difference in the pressure melting temperature expected by a reduction in overburden pressure (Fig. 1). These high gradient features also provide a means to shelter the frazil from potentially strong sub-ice currents (Soderlund *et al.* 2020), allowing crystals to accumulate and consolidate, forming marine ice. This process is analogous to the infilling of rifts at the Nansen and Roi Baudouin Ice Shelves by marine ice (Fig. 4). The texture of the NIS core was not columnar, suggesting no congelation growth had occurred within the rift (Khazendar *et al.* 2001).

This suggests the infilling of high gradient features in the ice shells of ocean worlds would likely be dominated by marine ice, as opposed to congelation ice, by nature of both the localized ice pump and the relatively low temperature gradients expected near the base of the ice shell. In this case, the salinity profile will likely decrease with depth within the consolidated layer. At the permeable-impermeable boundary, the salinity may appear to level off before increasing again as the brine volume fraction increases with depth (Fig. 4).

6. **Implications of Accretion at the Ice-Ocean Interface**

6.1. Geophysical Implications of Heterogeneous Accretion

The accretion of marine ice within basal features in a congelation ice shell has significant implications for processes governing surface-ice-ocean exchange. Marine ice accretion serves as a vehicle to deliver both sensible heat (by nature of its buoyant accumulation at the ice-ocean interface) and latent heat (generated by interstitial freezing of brine in the process of consolidation) into the ice shell interior. The infilling of these features by more ductile marine ice could affect the mechanical properties of the ice shell. Accretion in pre-existing fractures could facilitate strike-slip and lateral displacement, thought to be responsible for the linea observed on Europa's surface (Hammond 2020; Hoppa 1999; Hoppa *et al.* 2000; Prockter *et al.* 2000). The enhanced ductility would increase the Rayleigh number (ratio of buoyancy to diffusion), influencing convective vigor and modulating its responses to tidal forcing. This suggests marine ice accretion could also play a role in transitioning between convective and conductive regimes in an ice shell. The marine ice infilling these features is not only warmer but could also be significantly purer than the native ice shell material (see Table 2). As such marine ice is also compositionally buoyant, which could further promote the formation of narrow diapirs thought to be responsible for forming Europa's domes (Pappalardo and Barr 2004). Soderlund *et al.* (2013) proposed that marine ice accretion on regional scales, modulated by thickness gradients established by heterogeneous ocean-driven heating, could play a role in the formation of chaos terrain through a similar mechanism (Schmidt *et al.* 2011). Because of the timescales of tidal cycles on Enceladus, it is unlikely a highly-consolidated marine ice would be able to form within the tiger stripes; however, the formation and accumulation of frazil in the fissures, which would both generate latent heat and be capable of introducing a lag, may contribute to sustaining and modulating eruptions, a role previously attributed to turbulent dissipation alone (Kite and Rubin 2016).

6.2. Fractionation

The mode of salt entrapment, whether salt is accommodated within the ice lattice or interstitially as brine pockets, can influence the ice shell composition. A cellular interface would be more favorable for the entrainment of brine pockets than a planar interface, resulting in a bulk ice composition more representative of the underlying ocean in terms of the *relative* concentrations of major ionic species. Published studies of accreted ice chemistry (Table 3) broadly suggests that the chemical fractionation in sea and marine ice is minor and the differences between the mass ratios of ions in ice and seawater are on the order of 10^{-2}. There does not appear to be any evidence that sulfate or calcium are consistently either enriched or depleted in sea ice, although potassium appears to be depleted across all sea ice samples presented in Table 3. This is consistent with the idea that the degree of fractionation should scale with ion diffusivity (Maus *et al.* 2011) because potassium represents the fastest diffusing ion and thus is more efficiently removed from the ice through networks of brine channels.

The consistent enrichment of magnesium observed in sea ice (Table 3), cannot be attributed to known cryohydrate precipitation and is likely related to its slow diffusivity relative to chloride (Granskog *et al.* 2004; Maus *et al.* 2011). This suggests an enrichment of magnesium may be present in the ice shell, which supports the hypothesis put forth by Brown and Hand (2013) that magnesium salts from the ocean contribute to the radiolytic formation of magnesium sulfate salts at the surface of Europa. Although calcium and sulfate are also slow diffusing relative to chloride, these ions participate in cryohydrate formation early-on in sea ice growth (T > –8 °C) which could further influence the fractionation signal in an ice shell. If the ice becomes impermeable at a temperature above which any cryohydrates precipitate, then the composition of the ice should not differ significantly from that of the sub-ice ocean. If cryohydrates were to precipitate in a permeable medium, there is the potential that flushing from draining brine or melt could remove these impurities from the ice. The few studies of multi-year sea ice cores (Anderson and Jones 1985; Gjessing *et al.* 1993; Reeburgh and Springer-Young 1983) and the evolution of fractionation with depth observed in young sea ice cores (Maus *et al.* 2011) suggests the fractionation signal in young sea ice may not be preserved as the ice thickens and ages. The mixing model of Reeburgh and Springer-Young (1983) suggests that melt produced from warming as the ice ages removes ionic species conservatively; however, the sea ice samples of Gjessing *et al.* (1993) show strong sulfate depletion due to washout from melting snow.

TABLE 3. Fractionation reported in samples of sea ice and marine ice. Enrichment (+) and depletion (–) is taken in reference to what is observed in seawater. Where the fractionation is described as equal (=), the relative composition is considered to be within the uncertainty of seawater. Where the fractionation is described as (+/–), some ice cores analyzed in the study were enriched whereas others were depleted depending on sampling location. Where the fractionation is described as (=/–), the samples broadly suggested relative depletion, but the signal was not consistent across all depths. The fractionation presented for Maus *et al.* (2011) corresponds to that of the bulk ice. The marine ice sample in Warren *et al.* (1993) corresponds to the basal ice from Amery Ice Shelf. Ice type follows the same coding described in Fig. 4 (CS: Congelation Sea Ice, M: Marine Ice).

Ice Type	Ca/Cl	K/Cl	SO_4/Cl	Na/Cl	Mg/Cl	Source
CS	–	–	+	=	+	(Addison 1977)
CS	N/A	N/A	+/–	N/A	N/A	(Reeburgh and Springer-Young 1983)
CS	–	N/A	+/–	N/A	N/A	(Anderson and Jones 1985)
CS	=	–	=	=	+	(Meese 1989)
CS	=	N/A	–	=	=	(Gjessing *et al.* 1993)
CS	+	–	+	=	+	(Granskog *et al.* 2004)
CS	=	–	–	+	–	(Maus *et al.* 2011)
M	=	+	–	=	–	(Warren *et al.* 1993)
M	=/–	=/–	–	–	–	(Moore *et al.* 1994)
M	N/A	N/A	N/A	N/A	–	(Koch *et al.* 2015)

In a purely diffusive mode of salt entrapment, only impurities which are soluble in the ice lattice, such as chloride, would be incorporated in the ice shell. Because chloride can be accommodated in the lattice, it can be preserved in the ice as other insoluble ions retained in interstitial brine are rejected (Moore *et al.* 1994). This can be observed in samples of marine ice, where the degree of fractionation appears to increase as brine volume fraction and salinity decreases (Moore *et al.* 1994). Equilibrium freezing of the oceans presented in Table 1 would result in an ice chlorinity below the lattice solubility limit. This implies the chlorides incorporated in the ice could be entirely accommodated in the lattice. If the interstitial accommodation of impurities is minimal, this implies the ice shells of Europa and Enceladus should be enriched in chlorides. This indicates that although chloride salts have been observed on the surface and are correlated with endogenous features (Trumbo *et al.* 2019), this does not necessarily imply that the ocean is dominantly composed of chloride salts. Vance *et al.* (2019) also suggest that an ocean rich in sulfates may not be reflected in Europa's surface composition, although they attribute this to the preferential fractionation of sulfate predicted by FREZCHEM and observed in the multiyear ice cores of Gjessing *et al.* (1993) and Maus *et al.* (2011).The drainage and subsequent refreezing of melt will likely play an important role in redistributing sulfate in the ice shell, generating regions of local sulfate depletion and enrichment, respectively (Gjessing *et al.* 1993). Where marine ice accretion occurs, chloride enrichment will decrease with depth, inversely correlated to salinity and brine volume fraction.

6.3. Astrobiological Implications

Constraining the detailed physical structure and chemical characteristics of planetary ices have important implications for potential ice-ocean habitats. In terrestrial analog environments the porous, gradient rich ice-ocean interface provides a metabolically favorable substrate for a diverse array of aquatic organisms (Loose *et al.* 2011; Tedesco and Vichi 2014) and governs the biogeochemistry of the overlying ice (Brown *et al.* 2020; Buffo *et al.* 2019; Buffo *et al.* 2020; Schmidt 2020). In icy world systems (e.g., Europa, Enceladus), the stratigraphic and structural evolution of the ice shell, including porosity, temperature, and chemistry, will determine the spatial habitability of the respective cryosphere and determine the preservation/degradation of biosignatures as they are transported through the ice shell (Schmidt 2020). Water availability and water activity are two important metrics which strongly influence the ability of organisms to persist in extreme environments (Oren 2008; Tosca *et al.* 2008). Understanding the eutectic behavior of planetary ice shells, which is directly dependent on the ice's composition, will improve habitability estimates for ice-ocean worlds by constraining liquid fraction estimates as well as predictions of interstitial brine chemistry and water activity.

An additional constraint on biological viability as well as biosignature preservation is the chaotropicity and kosmostropicity of fluids within the shell. A measure of the tendency for solutes to stabilize (kosmotropes) or destabilize (chaotropes) proteins and membranes, chao-/kosmo-tropicity impacts the habitability of brines and could limit the survivability of detectable biosignatures as they are transported through the ice shell and subjected to thermal cycling (Hallsworth *et al.* 2007; Oren 2013; Pontefract *et al.* 2017). In many naturally occurring, charge balanced systems, the presence of kosmostropes offsets the destabilizing nature of chaotropes (e.g., seawater); however, if ions are preferentially fractionated through freezing or precipitation reactions, this balance can be upset and lead to toxic chaotropic solutions (Brown *et al.* 2020; Pontefract *et al.* 2017). One notable chaotrope is chloride (Cl^-), suggesting that an amplified presence in an ice shell due to fractionation could potentially spell disaster for resident biology if concentrations are high enough (Fox-Powell *et al.* 2016). The ice salinity and fractionation thus play an important role in determining the contemporary habitability of the ice shell as well as controlling the preservation of relict biosignatures. As such, constraining the ice-ocean interface dynamics—which govern the solute entrainment within and biogeochemical evolution of the shell—is an imperative part of assessing the habitability of ice-ocean worlds and designing life detection missions (Council 2011; Des Marais *et al.* 2008; Hendrix *et al.* 2019)

6.4. Implications for In Situ Detection of Biosignatures

The mechanism of accretion is known to influence the presence and entrainment of biosignatures in sea ice. Studies of sea ice have shown that its structure influences the concentration of biosignatures (specifically chlorophyll-a) in ice (Clarke and Ackley 1984; Garrison *et al.* 1983; Garrison *et al.* 1989). Chlorophyll-a has been used as a proxy for algal biomass in ice for decades (Meiners *et al.* 2018) and can be concentrated in the ice relative to the source water mechanically or by reproduction in the ice. These studies found that biological material was more concentrated in frazil ice than congelation ice due to mechanical incorporation driven by the buoyant consolidation of frazil ice crystals; however, the brine channels present in congelation ice serve as a pathway for nutrient exchange that may promote large algal blooms near the ice-water interface (Clarke and Ackley 1984). Although the brine channels that form in sea ice are recognized as a significant cryosphere habitat (Arrigo 2014; Loose *et al.* 2011), the ice must maintain sufficient permeability to enable nutrient exchange in support of maintaining these habitats. The cool, impermeable sea ice interior represents a less favorable environment for organisms (Arrigo 2014). This could translate to a reduced concentration of preserved biosignatures in the ice interior if organisms migrate with brine and are not trapped within brine pockets.

The unique ability of frazil ice to scavenge material as it accumulates is significant to biosignature entrainment and sampling (Arrigo *et al.* 2010; Garrison *et al.* 1989; Reimnitz *et al.* 1993). A notable example of these scavenging capabilities can be observed in McMurdo Sound, where benthic fauna, mobilized by anchor ice, have been found at the surface of the ice shelf (Dayton *et al.* 1969; Gow *et al.* 1965). There have not been many dedicated studies examining the incorporation of biosignatures in marine ice; however, one study of protists in the marine ice of Amery Ice Shelf revealed that these organisms were likely sourced from melting sea ice in the neighboring bay and were entrained in the ice as the meltwater was transported beneath the ice shelf (Roberts *et al.* 2006). This is significant because although marine ice did not serve as the original habitat to these organisms, it could incorporate and preserve these life forms even in the uppermost portion of the ice. This suggests that if life is present in the source water where frazil ice forms, biosignatures will likely be entrained as the frazil rises buoyantly to accumulate and consolidate at the ice-ocean interface. Because the marine ice is also buoyant relative to the surrounding ice shell, it can serve as a vehicle to deliver samples towards the surface where they might be sampled by a lander. Features associated with conditions favorable to the accretion of marine ice can thus serve as promising sites for in situ investigations searching for signs of life.

6.5. Implications for Radio Frequency (RF) Remote Sensing

The entrainment of oceanic material at the ice-ocean interface is an important consideration for remote instruments investigating the habitability of icy ocean worlds. The upcoming Europa Clipper (Howell and Pappalardo 2020) and JUICE (Grasset *et al.* 2013) missions are both equipped with ice-penetrating radar (IPR) instruments which will measure energy reflected from contrasts in the dielectric properties (e.g., electrical conductivity) within the ice shells of Jovian moons (Blankenship *et al.* 2009). The temperature, composition, and salinity will govern the brine volume fraction within the ice shell, generating eutectic interfaces that represent potential internal reflectors (Culha *et al.* 2020; Heggy *et al.* 2017). The temperature and concentration of lattice soluble impurities, such as chloride, will govern RF attenuation in ice, critical to both the signal penetration depth for IPR (Kalousová *et al.* 2017; Moore 2000) and in-ice remote communication for a cryobot (Dachwald *et al.* 2020). Dielectric contrasts generated by layers of hydrated salts or ice of different salinities also represent potential radar reflectors within the ice shell (Pettinelli *et al.* 2015).

Fluctuations in ice shell growth rates have the potential to generate layers of different salinities in a congelation ice shell. Peddinti and McNamara (2019) predict an increase in growth rate from 5.67 km/Myr to 8.22 km/Myr associated with the merging of convective cells within Europa's ice shell, which translates to growth velocities of 1.8×10^{-8} to 2.6×10^{-8} cm/s. At Enceladus, observed topographic anomalies are thought to be maintained by melting/freezing on the order of mm/yr (Čadek *et al.* 2019), which translates to growth velocities on the order of 10^{-9} cm/s. These growth velocities are comparable to the critical growth velocity at which an ice-water interface becomes planar for a terrestrial ocean (Wettlaufer 1992). If the transition in growth velocity modeled by Peddinti and McNamara (2019) is such that the ice-water interface stability is affected, this could result in a salinity contrast of up to an order of magnitude associated with this event (Fig. 5). A similar magnitude salinity contrast could be generated by the local and regional accretion of marine ice beneath congelation ice. These transitions in chlorinity represent dielectric contrasts that may be detectable by ice-penetrating radar.

7. **Conclusions**

Figure 6 summarizes the scenarios in which accreted ice can form on ocean worlds and provides some constraints regarding their properties. We have demonstrated that the critical factors governing the bulk salinity at the conditions expected at the ice-ocean interfaces of icy ocean worlds are the mechanism of accreted ice formation (frazil vs. congelation) and the microstructural interface geometry (planar vs. cellular).

Effective solute distribution coefficients (the ratio of ice salinity to source water salinity) derived from terrestrial ice cores and experimental results, allow us to constrain the bulk salinity of an ice shell formed through congelation growth (directional freezing from an existing interface) to be ~1% to ~10% of the ocean salinity. The upper bound distribution coefficient derived from sub-ice-shelf congelation ice cores, $k_{eq} = 6.7 \times 10^{-2}$, incorporates salt by the entrapment of brine pockets, which would occur if the interface retained a cellular microstructure, with characteristics consistent with terrestrial sea ice and sub-ice-shelf congelation ice. The lower bound distribution coefficient, $k_{eq} = 2.7 \times 10^{-3}$, reflects a purely diffusive mode of salt entrapment, corresponding to growth conditions where a planar ice-ocean interface is stable derived from experimental studies. As such, this distribution coefficient will only apply to salts that are soluble within the ice lattice, specifically chloride. If the salinity of the ice exceeds the lattice solubility limit for the lower bound distribution coefficient, any residual salts will be accommodated along grain boundaries and the lower bound distribution coefficient will increase to $k_{eq} = 4.7 \times 10^{-3}$.

A congelation ice shell may not be significantly compositionally fractionated relative to the sub-ice ocean in a bulk sense, although sea ice analogs suggest the degree of fractionation for a particular ion likely scales with its diffusivity (i.e., ions with higher diffusivity are more depleted) and that magnesium may be enriched. Where melting and refreezing occurs, the shell will show evidence of local enrichment and depletion of certain species. Low diffusivity species, such as sulfates, may show enhanced fractionation relative to other ions although this effect will be modulated by precipitation of cryohydrates. Over timescales relevant to the age of the ice shell, diffusion could redistribute impurities such that the ice shell fractionation scales with both age and the mobility of impurities, provided sufficient permeability and concentration gradients are maintained. If interstitial salts are preferentially removed, the ice shell will be enhanced in chlorides. An enrichment of chlorides could challenge the habitability of brine and preservation of biosignatures within the ice shell.

Locations where frazil ice forms, such as in rifts and basal crevasses serve as promising targets for sampling potential biosignatures entrained from the ocean. The accumulation and consolidation of frazil ice within these features will form marine ice, introducing relatively pure ice, $k_{eq} = 6.7 \times 10^{-4}$, into the interior with salinities ~0.1% of the ocean salinity. The accretion of marine ice will deliver both heat and relatively pure ice into the ice shell interior, introducing density anomalies that could support the formation of buoyant upwellings. The composition of the marine ice will become progressively enriched in chlorides as salinity and brine volume fraction decreases and the lattice solubility limit is approached.

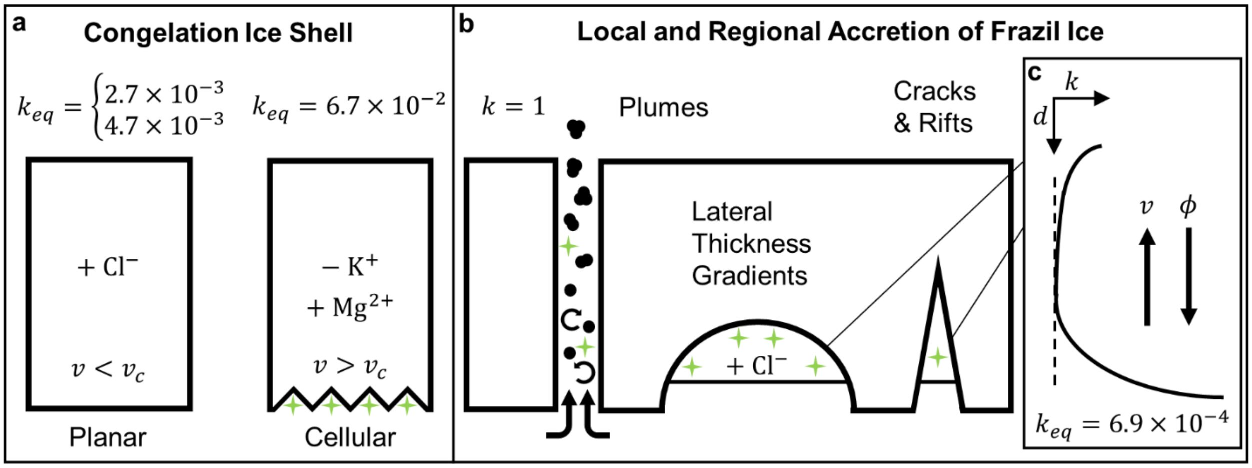

FIG. 6. Sketch depicting bulk properties of **(a)** a congelation ice shell which formed in the growth velocity regime where $k \approx k_{eq}$, **(b)** frazil ice accreting in local and regional features, and **(c)** a profile of depth vs. solute distribution coefficient inspired by the salinity profiles of marine ice presented in Fig. 4. v represents the growth velocity of the ice, v_c is the critical growth velocity at which a planar ice water interface becomes unstable, k is the effective solute distribution coefficient, d refers to the depth from the accretion interface, and ϕ is the melt fraction of the ice. The $+/-$ in (a) depicts enrichment and depletion of impurities in the ice, respectively. Properties are derived from studies of terrestrial accreted ice summarized in this work. The planar distribution coefficients assume a chloride solution. The lower bound assumes all chlorides are accommodated in the ice lattice, whereas the upper bound allows for some interstitial accommodation of impurities. The plume represented in (b) shows the nucleation of frazil in the turbulent water column as it as ascends and agglomerates. The green stars represent possible locations of biosignatures. A congelation ice shell with a cellular interface is more favorable for biosignature entrainment than a planar interface. Frazil ice would allow the incorporation of biosignatures through scavenging extending from the location where the frazil ice nucleates to the ice-ocean interface where it accretes.

The accretion of ice at the ice-ocean interface will govern the entrainment of oceanic material in the ice shell and serves as the primary filter controlling fingerprints of the ocean observable at the surface, including the relative concentration of major ionic species as well as biosignatures. The composition and bulk salinity of the ice shell will be important in governing the distribution and habitability of in-ice brine systems, which represent potential reflectors for ice-penetrating radar (IPR). The concentration of lattice soluble salts will influence the in-ice attenuation of radio frequency (RF) signals, significant to communication system design for a cryobot and penetration depth for IPR. Transitions in chlorinity represent dielectric contrasts, which may be detectable by ice-penetrating radar. Heterogeneous accretion can introduce buoyancy anomalies, which may promote local or regional geologic activity.

Terrestrial accreted ice can serve as an analog for accreted ice on ocean worlds. Studies of terrestrial accreted ice can support verification and validation of planned and future missions to icy ocean worlds and serve to constrain the parameter space and detection limits for in situ and remote instrument design. Future work should leverage natural samples of these ices for improved characterization of thermal, mechanical, and electrical properties in support of these missions.

Acknowledgements

N. S. W. was supported by the G. Unger Vetlesen Foundation and the Zonta International Amelia Earhart Fellowship. K. M. S. was supported by NASA grant NNX14AR28G. D. D. B. was supported by the G. Unger Vetlesen Foundation. This work benefited immensely from correspondence with Lisa Craw, Sönke Maus, Natalie Robinson, Yosef Ashkenazy, and John C. Moore. The authors declare that they have no known competing financial interests or personal relationships which have or could be perceived to have influenced the work reported in this paper.

References

Addison J. R. (1977) Impurity Concentrations In Sea Ice. *Journal of Glaciology*, 18: 117-127.

Anderson J., Schubert G., Jacobson R., Lau E., Moore W., and Sjogren W. (1998) Europa's differentiated internal structure: Inferences from four Galileo encounters. *Science*, 281: 2019-2022.

Anderson L. G., and Jones E. P. (1985) Measurements of total alkalinity, calcium, and sulfate in natural sea ice. *Journal of Geophysical Research: Oceans*, 90: 9194-9198.

Arrigo K. R. (2014) Sea ice ecosystems. *Annual Review of Marine Science*, 6: 439-467.

Arrigo K. R., Mock T., and Lizotte M. P. (2010) Primary producers and sea ice. *Sea ice*, 2: 283-325.

Ashkenazy Y. (2019) The surface temperature of Europa. *Heliyon*, 5: e01908.

Ashkenazy Y., Sayag R., and Tziperman E. (2018) Dynamics of the global meridional ice flow of Europa’s icy shell. *Nature Astronomy*, 2: 43-49.

Běhounková M., Souček O., Hron J., and Čadek O. (2017) Plume activity and tidal deformation on Enceladus influenced by faults and variable ice shell thickness. *Astrobiology*, 17: 941-954.

Billings S. E., and Kattenhorn S. A. (2005) The great thickness debate: Ice shell thickness models for Europa and comparisons with estimates based on flexure at ridges. *Icarus*, 177: 397-412.

Blankenship D. D., Young D. A., Moore W. B., and Moore J. C. (2009) Radar sounding of Europa’s subsurface properties and processes: The view from Earth. In: *Europa*, Univ. of Ariz. Press Tucson, pp 631-654.

Brown E. K., Buffo J. J., Grantham M., Pontefract A., Glass J., Ingall E., Doran P., Toubes-Rodrigo M., Dion-Kirschner H., and Carr C. (2020) Trapped in the Ice: An Analysis of Brines in British Columbia's Hypersaline Lakes. *LPI*: 2218.

Brown M., and Hand K. (2013) Salts and radiation products on the surface of Europa. *The Astronomical Journal*, 145: 110.

Brown M. E. (2001) Potassium in Europa's Atmosphere. *Icarus*, 151: 190-195.

Buffo J., Schmidt B., and Huber C. (2018) Multiphase reactive transport and platelet ice accretion in the sea ice of McMurdo sound, Antarctica. *Journal of Geophysical Research: Oceans*, 123: 324-345.

Buffo J., Schmidt B. E., Pontefract A., and Lawrence J. (2019) Frozen Fingerprints: Chemical and Biological Entrainment in Planetary Ices (Screen 6).Astrobiology Science Conference. AGU.

Buffo J. J., Schmidt B. E., Huber C., and Walker C. C. (2020) Entrainment and Dynamics of Ocean-derived Impurities within Europa's Ice Shell. *Journal of Geophysical Research: Planets*.

Burton J. A., Prim R. C., and Slichter W. P. (1953) The distribution of solute in crystals grown from the melt. Part I. Theoretical. *The journal of chemical physics*, 21: 1987-1991.

Čadek O., Souček O., Běhounková M., Choblet G., Tobie G., and Hron J. (2019) Long-term stability of Enceladus' uneven ice shell. *Icarus*, 319: 476-484.

Čadek O., Tobie G., Van Hoolst T., Massé M., Choblet G., Lefèvre A., Mitri G., Baland R. M., Běhounková M., Bourgeois O. and others. (2016) Enceladus's internal ocean and ice shell constrained from Cassini gravity, shape, and libration data. *Geophysical Research Letters*, 43: 5653-5660.

Carlson R., Anderson M., Mehlman R., and Johnson R. (2005) Distribution of hydrate on Europa: Further evidence for sulfuric acid hydrate. *Icarus*, 177: 461-471.

Cherepanov N. V. (1964) Structure of Sea Ice of Great Thickness. *Problems of Arctic Ice Research*, 267: 13-18.

Clarke D. B., and Ackley S. F. (1984) Sea ice structure and biological activity in the Antarctic marginal ice zone. *Journal of Geophysical Research: Oceans*, 89: 2087-2095.

Coriell S. R., McFadden G. B., and Sekerka R. F. (1985) Cellular growth during directional solidification. *Annual Review of Materials Science*, 15: 119-145.

Council N. R. (2011) Vision and Voyages for Planetary Science in the Decade 2013-2022. The National Academies Press, Washington, DC.

Cox G. F. N., and Weeks W. F. (1975) Brine drainage and initial salt entrapment in sodium chloride ice.

Cox G. F. N., and Weeks W. F. (1983) Equations for determining the gas and brine volumes in sea-ice samples. *Journal of Glaciology*, 29: 306-316.

Cox G. F. N., and Weeks W. F. (1988) Numerical simulations of the profile properties of undeformed first-year sea ice during the growth season. *Journal of Geophysical Research: Oceans*, 93: 12449-12460.

Craft K., and Roberts J. Fracture formation post impact on Enceladus?

Craft K. L., Patterson G. W., Lowell R. P., and Germanovich L. (2016) Fracturing and flow: Investigations on the formation of shallow water sills on Europa. *Icarus*, 274: 297-313.

Craven M., Allison I., Brand R., Elcheikh A., Hunter J., Hemer M., and Donoghue S. (2004) Initial borehole results from the Amery Ice Shelf hot-water drilling project. *Annals of Glaciology*, 39: 531-539(9).

Craven M., Allison I., Fricker H., and Warner R. (2009) Properties of a marine ice layer under the Amery Ice Shelf, East Antarctica. *Journal of Glaciology*, 55: 717-728(12).

Craw L. (2020) The Ice Shelf Lasagne: Understanding the Effects of Differing Rheologies on the Dynamics of an Ice Shelf, Abstract C015-07.AGU Fall Meeting.

Crawford G. D., and Stevenson D. J. (1988) Gas-driven water volcanism and the resurfacing of Europa. *Icarus*, 73: 66-79.

Culha C., Schroeder D. M., Jordan T. M., and Haynes M. S. (2020) Assessing the detectability of Europa's eutectic zone using radar sounding. *Icarus*, 339: 113578.

Dachwald B., Ulamec S., Postberg F., Sohl F., de Vera J.-P., Waldmann C., Lorenz R. D., Zacny K. A., Hellard H., and Biele J. (2020) Key technologies and instrumentation for subsurface exploration of ocean worlds. *Space Science Reviews*, 216: 1-45.

Daly S. F. (1984) Frazil Ice Dynamics. In: *CRREL Monograph*, U.S. Army Cold Regions Research and Engineering Laboratory, pp 56.

Dayton P. K., Robilliard G. A., and Devries A. L. (1969) Anchor Ice Formation in McMurdo Sound, Antarctica, and Its Biological Effects. *Science*, 163: 273-274.

Dempsey D. E., Langhorne P. J., Robinson N. J., Williams M. J. M., Haskell T. G., and Frew R. D. (2010) Observation and modeling of platelet ice fabric in McMurdo Sound, Antarctica. *Journal of Geophysical Research*, 115: 1-16.

Des Marais D. J., Nuth Iii J. A., Allamandola L. J., Boss A. P., Farmer J. D., Hoehler T. M., Jakosky B. M., Meadows V. S., Pohorille A., and Runnegar B. (2008) The NASA astrobiology roadmap. *Astrobiology*, 8: 715-730.

Dierckx M., and Tison J. L. (2013) Marine ice deformation experiments: an empirical validation of creep parameters. *Geophysical research letters*, 40: 134-138.

Drebushchak V. A., Drebushchak T. N., Ogienko A. G., and Yunoshev A. S. (2019) Crystallization of sodium chloride dihydrate (hydrohalite). *Journal of Crystal Growth*, 517: 17-23.

Eicken H. (1992) Salinity profiles of Antarctic sea ice: Field data and model results. *Journal of Geophysical Research: Oceans*, 97: 15545-15557.

Eicken H. (1998) Antarctic Research Series. In: *Deriving Modes and Rates of Ice Growth in the Weddell Sea from Microstructural, Salinity, and Stable-Isotope Data*, pp 89-122.

Eicken H. (2003) From the microscopic, to the macroscopic, to the regional scale: growth, microstructure and properties of sea ice. *Sea ice: an introduction to its physics, chemistry, biology and geology*: 22-81.

Eicken H., and Lange M. A. (1989) Development and properties of sea ice in the coastal regime of the southeastern Weddell Sea. *Journal of Geophysical Research: Oceans*, 94: 8193-8206.

Eicken H., Oerter H., Miller H., Graf W., and Kipfstuhl J. (1994) Textural characteristics and impurity content of meteoric and marine ice in the Ronne Ice Shelf, Antarctica. *Journal of Glaciology*, 40: 386-398.

Ettema R., Karim M. F., and Kennedy J. F. (1984) Laboratory experiments on frazil ice growth in supercooled water. *Cold Regions Science and Technology*, 10: 43-58.

Feltham D. L., Untersteiner N., Wettlaufer J. S., and Worster M. G. (2006) Sea ice is a mushy layer. *Geophysical Research Letters*, 33.

Fischer P. D., Brown M. E., and Hand K. P. (2015) Spatially resolved spectroscopy of Europa: The distinct spectrum of large-scale chaos. *The Astronomical Journal*, 150: 164.

Fitzsimons S., Mager S., Frew R., Clifford A., and Wilson G. (2012) Formation of ice-shelf moraines by accretion of sea water and marine sediment at the southern margin of the McMurdo Ice Shelf, Antarctica. *Annals of Glaciology*, 53: 211-220(10).

Foldvik A., and Kvinge T. Conditional instability of sea water at the freezing point. 21: 169-174.

Fox-Powell M. G., and Cousins C. R. (2021) Partitioning of Crystalline and Amorphous Phases During Freezing of Simulated Enceladus Ocean Fluids. *Journal of Geophysical Research: Planets*, 126: e2020JE006628.

Fox-Powell M. G., Hallsworth J. E., Cousins C. R., and Cockell C. S. (2016) Ionic strength is a barrier to the habitability of Mars. *Astrobiology*, 16: 427-442.

Garrison D. L., Ackley S. F., and Buck K. R. (1983) A physical mechanism for establishing algal populations in frazil ice. *Nature*, 306: 363-365.

Garrison D. L., Close A. R., and Reimnitz E. (1989) Algae concentrated by frazil ice: evidence from laboratory experiments and field measurements. *Antarctic Science*, 1: 313-316.
Geissler P. E., Greenberg R., Hoppa G., Helfenstein P., McEwen A., Pappalardo R., Tufts R., Ockert-Bell M., Sullivan R., Greeley R. and others. (1998) Evidence for non-synchronous rotation of Europa. *Nature*, 391: 34869.
Gjessing Y., Hanssen-Bauer I., Fujii Y., Kameda T., Kamiyama K., and Kawamura T. (1993) Chemical Fractionation in Sea Ice and Glacier Ice. *Bulletin of Glacier Research*: 1-8.
Glein C., Postberg F., and Vance S. (2018) The geochemistry of enceladus: composition and controls. *Enceladus and the Icy Moons of Saturn*, 39.
Glein C. R., Baross J. A., and Waite Jr J. H. (2015) The pH of Enceladus' ocean. *Geochimica et Cosmochimica Acta*, 162: 202-219.
Golden K. M., Ackley S. F., and Lytle V. I. (1998) The Percolation Phase Transition in Sea Ice. *Science*, 282: 2238-2241.
Golden K. M., Eicken H., Heaton A. L., Miner J., Pringle D. J., and Zhu J. (2007) Thermal evolution of permeability and microstructure in sea ice. *Geophysical Research Letters*, 34.
Goodman J. C. (2018) Interactions Between Ocean Circulation and Topography in Icy Worlds. *LPICo*, 2085: 6048.
Gow A. J., Ackley S. F., Buck K. R., and Golden K. M. (1987) Physical and structural characteristics of Weddell Sea pack ice. In: *CRREL Report*, U.S. Army Cold Regions Research and Engineering Laboratory, pp 80.
Gow A. J., Ackley S. F., Govoni J. W., and Weeks W. F. (1998) Antarctic Research Series. In: *Physical and Structural Properties of Land-Fast Sea Ice in McMurdo Sound, Antarctica*, pp 355-374.
Gow A. J., and Epstein S. (1972) On the use of stable isotopes to trace the origins of ice in a floating ice tongue. *Journal of Geophysical Research*, 77: 6552-6557.
Gow A. J., and Langston D. (1977) Growth history of lake ice in relation to its stratigraphic, crystalline and mechanical structure. Department of Defense, Army, Corps of Engineers, Cold Regions Research and ….
Gow A. J., Weeks W. F., Hendrickson G., and Rowland R. (1965) New Light on the Mode of Uplift of the Fish and Fossiliferous Moraines of the Mcmurdo Ice Shelf, Antarctica. *Journal of Glaciology*, 5: 813-828.
Granskog M. A., Uusikivi J., Sequeiros A. B., and Sonninen E. (2006) Relation of ice growth rate to salt segregation during freezing of low-salinity sea water (Bothnian Bay, Baltic Sea). *Annals of Glaciology*, 44: 134-138.
Granskog M. A., Virkkunen K., Thomas D. N., Ehn J., Kola H., and Martma T. (2004) Chemical properties of brackish water ice in the Bothnian Bay, the Baltic Sea. *Journal of Glaciology*, 50: 292-302.
Grasset O., Dougherty M. K., Coustenis A., Bunce E. J., Erd C., Titov D., Blanc M., Coates A., Drossart P., and Fletcher L. N. (2013) JUpiter ICy moons Explorer (JUICE): An ESA mission to orbit Ganymede and to characterise the Jupiter system. *Planetary and Space Science*, 78: 1-21.
Greeley R., Sullivan R., Coon M. D., Geissler P. E., Tufts B. R., Head J. W., Pappalardo R. T., and Moore J. M. (1998) Terrestrial Sea Ice Morphology: Considerations for Europa. *Icarus*, 135: 25-40.

Greenberg R., Geissler P., Hoppa G., Tufts B. R., Durda D. D., Pappalardo R., Head J. W., Greeley R., Sullivan R., and Carr M. H. (1998) Tectonic Processes on Europa: Tidal Stresses, Mechanical Response, and Visible Features. *Icarus*, 135: 64-78.

Greene C. A., Gwyther D. E., and Blankenship D. D. (2017) Antarctic mapping tools for MATLAB. *Computers & Geosciences*, 104: 151-157.

Griewank P. J., and Notz D. (2013) Insights into brine dynamics and sea ice desalination from a 1-D model study of gravity drainage. *Journal of Geophysical Research: Oceans*, 118: 3370-3386.

Gross G., Wong P., and Humes K. (1977) Concentration dependent solute redistribution at the ice–water phase boundary. III. Spontaneous convection. Chloride solutions. *The Journal of Chemical Physics*, 67: 5264-5274.

Grothe S., Hughes K., and Langhorne P. (2014) 22nd IAHR International Symposium on Ice.

Hallsworth J. E., Yakimov M. M., Golyshin P. N., Gillion J. L. M., D'Auria G., de Lima Alves F., La Cono V., Genovese M., McKew B. A., and Hayes S. L. (2007) Limits of life in MgCl2-containing environments: chaotropicity defines the window. *Environmental Microbiology*, 9: 801-813.

Hammond N. P. (2020) Estimating the Magnitude of Cyclic Slip on Strike-Slip faults on Europa. *Journal of Geophysical Research: Planets*, 125: no-no.

Hammond N. P., Parmenteir E. M., and Barr A. C. (2018) Compaction and Melt Transport in Ammonia-Rich Ice Shells: Implications for the Evolution of Triton. *Journal of Geophysical Research: Planets*, 123: 3105-3118.

Hand K., and Carlson R. (2015) Europa's surface color suggests an ocean rich with sodium chloride. *Geophysical Research Letters*, 42: 3174-3178.

Hand K. P., and Chyba C. F. (2007) Empirical constraints on the salinity of the europan ocean and implications for a thin ice shell. *Icarus*, 189: 424-438.

Harrison J. D., and Tiller W. A. (1963) Ice interface morphology and texture developed during freezing. *Journal of Applied Physics*, 34: 3349-3355.

Heggy E., Scabbia G., Bruzzone L., and Pappalardo R. T. (2017) Radar probing of Jovian icy moons: Understanding subsurface water and structure detectability in the JUICE and Europa missions. *Icarus*, 285: 237-251.

Helfenstein P., and Parmentier E. M. (1985) Patterns of fracture and tidal stresses due to nonsynchronous rotation: Implications for fracturing on Europa. *Icarus*, 61: 175-184.

Hemingway D. J., and Mittal T. (2019) Enceladus's ice shell structure as a window on internal heat production. *Icarus*, 332: 111-131.

Hemingway D. J., Rudolph M. L., and Manga M. (2020) Cascading parallel fractures on Enceladus. *Nature Astronomy*, 4: 234-239.

Hendrix A. R., Hurford T. A., Barge L. M., Bland M. T., Bowman J. S., Brinckerhoff W., Buratti B. J., Cable M. L., Castillo-Rogez J., and Collins G. C. (2019) The NASA roadmap to ocean worlds. *Astrobiology*, 19: 1-27.

Hesse M. A., Jordan J. S., Vance S. D., and McCarthy C. (2020) Oxidant Transport Through Europa's Ice Shell by Brine Drainage from Chaotic Terrains. *LPI*: 3073.

Holland P. R., Corr H. F. J., Vaughan D. G., Jenkins A., and Skvarca P. (2009) Marine ice in Larsen Ice Shelf. *Geophysical Research Letters*, 36.

Hoppa G. (1999) Strike–Slip Faults on Europa: Global Shear Patterns Driven by Tidal Stress. *Icarus*, 141: 287-298.

Hoppa G., Greenberg R., Tufts B. R., Geissler P., Phillips C., and Milazzo M. (2000) Distribution of strike-slip faults on Europa. *Journal of Geophysical Research: Planets*, 105: 22617-22627.

Hoppmann M., Richter M. E., Smith I. J., Jendersie S., Langhorne P. J., Thomas D. N., and Dieckmann G. (2020) Platelet ice, the Southern Ocean's hidden ice: a review. *Annals of Glaciology*, 62.

Howell S. M., and Pappalardo R. T. (2018) Band Formation and Ocean-Surface Interaction on Europa and Ganymede. *Geophysical Research Letters*, 45: 4701-4709.

Howell S. M., and Pappalardo R. T. (2020) NASA's Europa Clipper—a mission to a potentially habitable ocean world. *Nature Communications*, 11: 1-4.

Hubbard B., Tison J.-L., Pattyn F., Dierckx M., Boereboom T., and Samyn D. (2012) Optical-televiewer-based identification and characterization of material facies associated with an Antarctic ice-shelf rift. *Annals of glaciology*, 53: 137-146.

Hunke E. C., Notz D., Turner A. K., and Vancoppenolle M. (2011) The multiphase physics of sea ice: A review. *Cryosphere*, 5: 989-1009.

Hurford T. A., Helfenstein P., Hoppa G. V., Greenberg R., and Bills B. G. (2007) Eruptions arising from tidally controlled periodic openings of rifts on Enceladus. *Nature*, 447: 292-294.

Iess L., Stevenson D. J., Parisi M., Hemingway D., Jacobson R. A., Lunine J. I., Nimmo F., Armstrong J. W., Asmar S. W., and Ducci M. (2014) The gravity field and interior structure of Enceladus. *Science*, 344: 78-80.

Jackson K. A. (2004) Constitutional supercooling surface roughening. *Journal of Crystal Growth*, 264: 519-529.

Jansen D., Luckman A., Kulessa B., Holland P. R., and King E. C. (2013) Marine ice formation in a suture zone on the Larsen C Ice Shelf and its influence on ice shelf dynamics. *Journal of Geophysical Research: Earth Surface*, 118: 1628-1640.

Jeffries M. O., Schwartz K., Morris K., Veazey A. D., Krouse H. R., and Gushing S. (1995) Evidence for platelet ice accretion in Arctic sea ice development. *Journal of Geophysical Research: Oceans*, 100: 10905-10914.

Jeffries M. O., Weeks W. F., Shaw R., and Morris K. (1993) Structural characteristics of congelation and platelet ice and their role in the development of antarctic land-fast sea ice. *Journal of Glaciology*, 39: 223-238.

Jia X., Kivelson M. G., Khurana K. K., and Kurth W. S. (2018) Evidence of a plume on Europa from Galileo magnetic and plasma wave signatures. *Nature Astronomy*, 2: 459-464.

Johnston S. A., and Montési L. G. J. (2017) The impact of a pressurized regional sea or global ocean on stresses on Enceladus. *Journal of Geophysical Research: Planets*, 122: 1258-1275.

Kalousová K., Schroeder D. M., and Soderlund K. M. (2017) Radar attenuation in Europa's ice shell: Obstacles and opportunities for constraining the shell thickness and its thermal structure. *Journal of Geophysical Research: Planets*, 122: 524-545.

Kalousová K., Souček O., Tobie G., Choblet G., and Čadek O. (2014) Ice melting and downward transport of meltwater by two-phase flow in Europa's ice shell. *Journal of Geophysical Research: Planets*, 119: 532-549.

Kargel J. S., Kaye J. Z., Head Iii J. W., Marion G. M., Sassen R., Crowley J. K., Ballesteros O. P., Grant S. A., and Hogenboom D. L. (2000) Europa's crust and ocean: origin, composition, and the prospects for life. *Icarus*, 148: 226-265.

Khazendar A., and Jenkins A. (2003) A model of marine ice formation within Antarctic ice shelf rifts. *Journal of Geophysical Research*, 108.

Khazendar A., Rignot E., and Larour E. (2009) Roles of marine ice, rheology, and fracture in the flow and stability of the Brunt/Stancomb-Wills Ice Shelf. *Journal of Geophysical Research: Earth Surface*, 114.

Khazendar A., Tison J. L., Stenni B., Dini M., and Bondesan A. (2001) Significant marine-ice accumulation in the ablation zone beneath an Antarctic ice shelf. *Journal of Glaciology*, 47: 359-368.

Kite E. S., and Rubin A. M. (2016) Sustained eruptions on Enceladus explained by turbulent dissipation in tiger stripes. *Proceedings of the National Academy of Sciences*, 113: 3972-3975.

Koch I., Fitzsimons S., Samyn D., and Tison J.-L. (2015) Marine ice recycling at the southern McMurdo Ice Shelf, Antarctica. *Journal of Glaciology*, 61: 689-701(13).

Kulessa B., Jansen D., Luckman A. J., King E. C., and Sammonds P. R. (2014) Marine ice regulates the future stability of a large Antarctic ice shelf. *Nature communications*, 5: 1-7.

Kvajić G., and Brajović V. (1971) Anisotropic segregation of (K+) by dendritic ice crystals. *Journal of Crystal Growth*, 11: 73-76.

Lange M. A. (1988) Basic Properties of Antarctic Sea Ice as Revealed by Textural Analysis of Ice Cores. *Annals of Glaciology*, 10: 95-101.

Lange M. A., Ackley S. F., Wadhams P., Dieckmann G. S., and Eicken H. (1989) Development of Sea Ice in the Weddell Sea. *Annals of Glaciology*, 12: 92-96.

Langhorne P. J., and Robinson W. H. (1986) Alignment of crystals in sea ice due to fluid motion. *Cold Regions Science and Technology*, 12: 197-214.

Lee S., Pappalardo R. T., and Makris N. C. (2005) Mechanics of tidally driven fractures in Europa's ice shell. *Icarus*, 177: 367-379.

Leliwa-Kopystyński J., Maruyama M., and Nakajima T. (2002) The water–ammonia phase diagram up to 300 MPa: Application to icy satellites. *Icarus*, 159: 518-528.

Leppäranta M. (2015) Structure and Properties of Lake Ice. In: *Freezing of Lakes and the Evolution of their Ice Cover*. edited by M Leppärantas, Springer Berlin Heidelberg, Berlin, Heidelberg, pp 51-90.

Lewis E. L., and Perkin R. G. (1981) The Practical Salinity Scale 1978: conversion of existing data. *Deep Sea Research Part A. Oceanographic Research Papers*, 28: 307-328.

Lewis E. L., and Perkin R. G. (1986) Ice pumps and their rates. *Journal of Geophysical Research: Oceans (1978–2012)*, 91: 11756-11762.

Lofgren G., and Weeks W. F. (1969) Effect of growth parameters on substructure spacing in NaCl ice crystals. *journal of Glaciology*, 8: 153-164.

Loose B., Miller L. A., Elliott S., and Papakyriakou T. (2011) Sea ice biogeochemistry and material transport across the frozen interface. *Oceanography*, 24: 202-218.

Mager S. M., Smith I. J., Kempema E. W., Thomson B. J., and Leonard G. H. (2013) Anchor ice in polar oceans. *Progress in Physical Geography*, 37: 468-483.

Makkonen L. (1987) Salinity and growth rate of ice formed by sea spray. *Cold Regions Science and Technology*, 14: 163-171.

Manga M., and Michaut C. (2017) Formation of lenticulae on Europa by saucer-shaped sills. *Icarus*, 286: 261-269.

Manga M., and Wang C. Y. (2007) Pressurized oceans and the eruption of liquid water on Europa and Enceladus. *Geophysical Research Letters*, 34.

Martin A., and McMinn A. (2018) Sea ice, extremophiles and life on extra-terrestrial ocean worlds. *International Journal of Astrobiology*, 17: 1-16.
Maus S. (2006) The planar-cellular transition during freezing of natural waters.11th International Conference on the Physics and Chemistry of Ice.
Maus S. (2007) On brine entrapment in sea ice: morphological stability, microstructure and convection. Logos-Verlag.
Maus S. (2020) The plate spacing of sea ice. *Annals of Glaciology*, 82.
Maus S., Müller S., Büttner J., Brütsch S., Huthwelker T., Schwikowski M., Enzmann F., and Vähätolo A. (2011) Ion fractionation in young sea ice from Kongsfjorden, Svalbard. *Annals of Glaciology*, 52: 301-310.
McCord T., Hansen G., Fanale F., Carlson R., Matson D., Johnson T., Smythe W., Crowley J., Martin P., and Ocampo A. (1998) Salts on Europa's surface detected by Galileo's near infrared mapping spectrometer. *Science*, 280: 1242-1245.
McCord T. B., Hansen G. B., Matson D. L., Johnson T. V., Crowley J. K., Fanale F. P., Carlson R. W., Smythe W. D., Martin P. D., and Hibbitts C. A. (1999) Hydrated salt minerals on Europa's surface from the Galileo near-infrared mapping spectrometer (NIMS) investigation. *Journal of Geophysical Research: Planets*, 104: 11827-11851.
McGrath D., Steffen K., Holland P. R., Scambos T., Rajaram H., Abdalati W., and Rignot E. (2014) The structure and effect of suture zones in the Larsen C Ice Shelf, Antarctica. *Journal of Geophysical Research: Earth Surface*, 119: 588-602.
McGuinness M. J., Williams M. J. M., Langhorne P. J., Purdie C., and Crook J. (2009) Frazil deposition under growing sea ice. *Journal of Geophysical Research: Oceans*, 114.
McKinnon W. B. (2015) Effect of Enceladus's rapid synchronous spin on interpretation of Cassini gravity. *Geophysical Research Letters*, 42: 2137-2143.
Meese D. A. (1989) The chemical and structural properties of sea ice in the southern Beaufort Sea. In: *CRREL Report*, U.S. Army Cold Regions Research and Engineering Laboratory, pp 144.
Meiners K. M., Vancoppenolle M., Carnat G., Castellani G., Delille B., Delille D., Dieckmann G. S., Flores H., Fripiat F., Grotti M. and others. (2018) Chlorophyll-a in Antarctic Landfast Sea Ice: A First Synthesis of Historical Ice Core Data. *Journal of Geophysical Research: Oceans*, 123: 8444-8459.
Michaut C., and Manga M. (2014) Domes, pits, and small chaos on Europa produced by water sills. *Journal of Geophysical Research: Planets*, 119: 550-573.
Moore J. C. (2000) Models of radar absorption in Europan ice. *Icarus*, 147: 292-300.
Moore J. C., Reid A. P., and Kipfstuhl J. (1994) Microstructure and electrical properties of marine ice and its relationship to meteoric ice and sea ice. *Journal of Geophysical Research: Oceans (1978–2012)*, 99: 5171-5180.
Morgan V. I. (1972) Oxygen Isotope Evidence for Bottom Freezing on the Amery Ice Shelf. *Nature*, 238: 393-394.
Mullins W. W., and Sekerka R. F. (1964) Stability of a planar interface during solidification of a dilute binary alloy. *Journal of applied physics*, 35: 444-451.
Nagashima K., and Furukawa Y. (1997) Solute distribution in front of an ice/water interface during directional growth of ice crystals and its relationship to interfacial patterns. *The Journal of Physical Chemistry B*, 101: 6174-6176.
Nakawo M., and Sinha N. K. (1981) Growth Rate and Salinity Profile of First-Year Sea Ice in the High Arctic. *Journal of Glaciology*, 27: 315-330.

Neal C. S. (1979) The Dynamics of the Ross Ice Shelf Revealed by Radio Echo-Sounding. *Journal of Glaciology*, 24: 295-307.

Nimmo F. (2004a) Non-Newtonian topographic relaxation on Europa. *Icarus*, 168: 205-208.

Nimmo F. (2004b) Stresses generated in cooling viscoelastic ice shells: Application to Europa. *Journal of Geophysical Research: Planets*, 109.

Nimmo F., and Bills B. G. (2010) Shell thickness variations and the long-wavelength topography of Titan. *Icarus*, 208: 896-904.

Nimmo F., Thomas P. C., Pappalardo R. T., and Moore W. B. (2007) The global shape of Europa: Constraints on lateral shell thickness variations. *Icarus*, 191: 183-192.

Notz D., and Worster M. G. (2009) Desalination processes of sea ice revisited. *Journal of Geophysical Research*, 114.

O'Neill C., and Nimmo F. (2010) The role of episodic overturn in generating the surface geology and heat flow on Enceladus. *Nature Geoscience*, 3: 88.

Oerter H., Kipfstuhl J., Determann J., Miller H., Wagenbach D., Minikin A., and Graft W. (1992) Evidence for basal marine ice in the Filchner–Ronne ice shelf. *Nature*, 358: 358399a0.

Ojakangas G., and Stevenson D. (1989) Thermal state of an ice shell on Europa. *Icarus*, 81: 220-241.

Oren A. (2008) Microbial life at high salt concentrations: phylogenetic and metabolic diversity. *Saline systems*, 4: 2.

Oren A. (2013) Life in magnesium-and calcium-rich hypersaline environments: salt stress by chaotropic ions. In: *Polyextremophiles*, Springer, pp 215-232.

Osterkamp T. E. (1977) Frazil-Ice Nucleation by Mass-Exchange Processes at the Air-Water Interface. *Journal of Glaciology*, 19: 619-627.

Osterkamp T. E., and Weber A. H. (1970) Electrical phenomena accompanying the phase change of dilute KCl solutions into single crystals of ice. *Journal of Glaciology*, 9: 269-277.

Palosuo E. (1961) Crystal structure of brackish and freshwater ice. *IASH*, 54: 14.

Pappalardo R. T., and Barr A. C. (2004) The origin of domes on Europa: The role of thermally induced compositional diapirism. *Geophysical Research Letters*, 31.

Patthoff D. A., Kattenhorn S. A., and Cooper C. M. (2019) Implications of nonsynchronous rotation on the deformational history and ice shell properties in the south polar terrain of Enceladus. *Icarus*, 321: 445-457.

Pattyn F., Matsuoka K., Callens D., Conway H., Depoorter M., Docquier D., Hubbard B., Samyn D., and Tison J. L. (2012) Melting and refreezing beneath Roi Baudouin Ice Shelf (East Antarctica) inferred from radar, GPS, and ice core data. *Journal of Geophysical Research: Earth Surface*, 117.

Peddinti D. A., and McNamara A. K. (2015) Material transport across Europa's ice shell. *Geophysical Research Letters*, 42: 4288-4293.

Peddinti D. A., and McNamara A. K. (2019) Dynamical investigation of a thickening ice-shell: Implications for the icy moon Europa. *Icarus*, 329: 251-269.

Petrich C., and Eicken H. (2017) Overview of sea ice growth and properties. In: *Sea Ice*. edited by DN Thomass, John Wiley & Sons, pp 1-41.

Petrich C., Langhorne P., and Eicken H. (2011) Modeled Bulk Salinity of Growing First-Year Sea Ice and Implications for Ice Properties in Spring.International Conference on Port and Ocean Engineering under Arctic Conditions, Montreal, Canada.

Petrich C., Langhorne P. J., and Sun Z. F. (2006) Modelling the interrelationships between permeability, effective porosity and total porosity in sea ice. *Cold Regions Science and Technology*, 44: 131-144.

Pettinelli E., Cosciotti B., Di Paolo F., Lauro S. E., Mattei E., Orosei R., and Vannaroni G. (2015) Dielectric properties of Jovian satellite ice analogs for subsurface radar exploration: A review. *Reviews of Geophysics*, 53: 593-641.

Pillay V., Gärtner R. S., Himawan C., Seckler M. M., Lewis A. E., and Witkamp G.-J. (2005) MgSO4+ H2O System at Eutectic Conditions and Thermodynamic Solubility Products of MgSO4⊙ 12H2O (s) and MgSO4⊙ 7H2O (s). *Journal of Chemical & Engineering Data*, 50: 551-555.

Pontefract A., Zhu T. F., Walker V. K., Hepburn H., Lui C., Zuber M. T., Ruvkun G., and Carr C. E. (2017) Microbial diversity in a hypersaline sulfate lake: a terrestrial analog of ancient Mars. *Frontiers in microbiology*, 8: 1819.

Postberg F., Clark R. N., Hansen C. J., Coates A. J., Dalle Ore C. M., Scipioni F., Hedman M. M., and Waite J. H. (2018) Plume and surface composition of Enceladus. *Enceladus and the Icy Moons of Saturn*: 129-162.

Postberg F., Schmidt J., Hillier J., Kempf S., and Srama R. (2011) A salt-water reservoir as the source of a compositionally stratified plume on Enceladus. *Nature*, 474: 620-2.

Priscu J. C., Fritsen C. H., Adams E. E., Giovannoni S. J., Paerl H. W., McKay C. P., Doran P. T., Gordon D. A., Lanoil B. D., and Pinckney J. L. (1998) Perennial Antarctic lake ice: an oasis for life in a polar desert. *Science*, 280: 2095-2098.

Prockter L. M., Pappalardo R. T., and Head Iii J. W. (2000) Strike-slip duplexing on Jupiter's icy moon Europa. *Journal of Geophysical Research: Planets*, 105: 9483-9488.

Reeburgh W. S., and Springer-Young M. (1983) New measurements of sulfate and chlorinity in natural sea ice. *Journal of Geophysical Research: Oceans*, 88: 2959-2966.

Reimnitz E., Clayton J. R., Kempema E. W., Payne J. R., and Weber W. S. (1993) Interaction of rising frazil with suspended particles: tank experiments with applications to nature. *Cold Regions Science and Technology*, 21: 117-135.

Rhoden A. R., Hurford T. A., and Manga M. (2011) Strike-slip fault patterns on Europa: Obliquity or polar wander? *Icarus*, 211: 636-647.

Rhoden A. R., Wurman G., Huff E. M., Manga M., and Hurford T. A. (2012) Shell tectonics: A mechanical model for strike-slip displacement on Europa. *Icarus*, 218: 297-307.

Roberts D., Craven M., Cai M., Allison I., and Nash G. (2006) Protists in the marine ice of the Amery Ice Shelf, East Antarctica. *Polar Biology*, 30: 143-153.

Robinson N. J., Grant B. S., Stevens C. L., Stewart C. L., and Williams M. J. M. (2019) Oceanographic observations in supercooled water: Protocols for mitigation of measurement errors in profiling and moored sampling. *Cold Regions Science and Technology*: 102954.

Rohatgi A. (2017) WebPlotDigitizer.

Rudolph M. L., and Manga M. (2009) Fracture penetration in planetary ice shells. *Icarus*, 199: 536-541.

Rutter J. W., and Chalmers B. (1953) A prismatic substructure formed during solidification of metals. *Canadian Journal of Physics*, 31: 15-39.

Schenk P., Matsuyama I., and Nimmo F. (2008) True polar wander on Europa from global-scale small-circle depressions. *Nature*, 453: 368.

Schilling N., Khurana K. K., and Kivelson M. G. (2004) Limits on an intrinsic dipole moment in Europa. *Journal of Geophysical Research: Planets (1991–2012)*, 109.

Schilling N., Neubauer F. M., and Saur J. (2007) Time-varying interaction of Europa with the jovian magnetosphere: Constraints on the conductivity of Europa's subsurface ocean. *Icarus*, 192: 41-55.

Schmidt B. E. (2020) The Astrobiology of Europa and the Jovian System. *Planetary Astrobiology*: 185.

Schmidt B. E., Blankenship D. D., Patterson G. W., and Schenk P. M. (2011) Active formation of ‘chaos terrain’ over shallow subsurface water on Europa. *Nature*, 479: 502.

Seidensticker R. G. (1972) Partitioning of HCl in the water-ice system. *The Journal of Chemical Physics*, 56: 2853-2857.

Sekerka R. F., Coriell S. R., and McFadden G. B. (2015) Morphological stability. In: *Handbook of Crystal Growth*, Elsevier, pp 595-630.

Shokr M., and Sinha N. (2015) Sea ice: physics and remote sensing. John Wiley & Sons.

Smith I. J., Langhorne P. J., Frew R. D., Vennell R., and Haskell T. G. (2012) Sea ice growth rates near ice shelves. *Cold regions science and technology*, 83: 57-70.

Smith I. J., Langhorne P. J., Haskell T. G., Trodahl H. J., Frew R., and Vennell M. R. (2001) Platelet ice and the land-fast sea ice of McMurdo Sound, Antarctica. *Annals of Glaciology*, 33: 21-27.

Soderlund K. M. (2019) Ocean dynamics of outer solar system satellites. *Geophysical Research Letters*, 46: 8700-8710.

Soderlund K. M., Kalousová K., Buffo J. J., Glein C. R., Goodman J. C., Mitri G., Patterson G. W., Postberg F., Rovira-Navarro M., and Rückriemen T. (2020) Ice-Ocean Exchange Processes in the Jovian and Saturnian Satellites. *Space Science Reviews*, 216: 1-57.

Soderlund K. M., Schmidt B. E., Wicht J., and Blankenship D. D. (2013) Ocean-driven heating of Europa's icy shell at low latitudes. *Nature Geoscience*, 7: 16-19.

Souchez R., Meneghel M., Tison J. L., Lorrain R., Ronveaux D., Baroni C., Lozej A., Tabacco I., and Jouzel J. (1991) Ice composition evidence of marine ice transfer along the bottom of a small Antarctic Ice Shelf. *Geophysical Research Letters*, 18: 849-852.

Souchez R., Petit J. R., Jouzel J., De Angelis M., and Tison J. L. (2004) Reassessing Lake Vostok’s behaviour from existing and new ice core data. *Earth and Planetary Science Letters*, 217: 163-170.

Souchez R., Tison J. L., and Jouzel J. (1988) Deuterium concentration and growth rate of Antarctic first-year sea ice. *Geophysical research letters*, 15: 1385-1388.

Sparks W. B., Schmidt B. E., McGrath M. A., Hand K. P., Spencer J. R., Cracraft M., and Deustua S. E. (2017) Active cryovolcanism on Europa? *The Astrophysical Journal Letters*, 839: L18.

Spencer J., Nimmo F., Ingersoll A. P., Hurford T., Kite E., Rhoden A., Schmidt J., and Howett C. (2018) Plume origins and plumbing: from ocean to surface. *Enceladus and the Icy Moons of Saturn*: 163.

Spencer J. R., Pearl J. C., Segura M., Flasar F. M., Mamoutkine A., Romani P., Buratti B. J., Hendrix A. R., Spilker L. J., and Lopes R. M. C. (2006) Cassini Encounters Enceladus: Background and the Discovery of a South Polar Hot Spot. *Science*, 311: 1401-1405.

Squyres S. W., Reynolds R. T., Cassen P. M., and Peale S. J. (1983) The evolution of Enceladus. *Icarus*, 53: 319-331.

Steinbrügge G., Voigt J. R. C., Wolfenbarger N. S., Hamilton C. W., Soderlund K. M., Young D. A., Blankenship D. D., Vance S. D., and Schroeder D. M. (2020) Brine Migration and Impact-Induced Cryovolcanism on Europa. *Geophysical Research Letters*, 47: e2020GL090797.

Tajeddine R., Soderlund K. M., Thomas P. C., Helfenstein P., Hedman M. M., Burns J. A., and Schenk P. M. (2017) True polar wander of Enceladus from topographic data. *Icarus*, 295: 46-60.

Tedesco L., and Vichi M. (2014) Sea ice biogeochemistry: A guide for modellers. *PloS one*, 9: e89217.

Terwilliger J. P., and Dizio S. F. (1970) Salt rejection phenomena in the freezing of saline solutions. *Chemical Engineering Science*, 25: 1331-1349.

Thomas D. N. (2017) Sea ice. John Wiley & Sons.

Thomas P. C., Tajeddine R., Tiscareno M. S., Burns J. A., Joseph J., Loredo T. J., Helfenstein P., and Porco C. (2016) Enceladus's measured physical libration requires a global subsurface ocean. *Icarus*, 264: 37-47.

Timco G. W., and Weeks W. F. (2010) A review of the engineering properties of sea ice. *Cold regions science and technology*, 60: 107-129.

Tison J. L., Khazendar A., and Roulin E. (2001) A two-phase approach to the simulation of the combined isotope/salinity signal of marine ice. *Journal of Geophysical Research: Oceans*, 106: 31387-31401.

Tison J. L., Lorrain R. D., Bouzette A., Dini M., Bondesan A., and StiéVenard M. (1998) Linking Landfast Sea Ice Variability to Marine Ice Accretion at Hells Gate Ice Shelf, Ross Sea. pp 375-407.

Tison J. L., Ronveaux D., and Lorrain R. D. (1993) Low salinity frazil ice generation at the base of a small Antarctic ice shelf. *Antarctic Science*, 5: 309-322.

Tobie G., Gautier D., and Hersant F. (2012) Titan's bulk composition constrained by Cassini-Huygens: implication for internal outgassing. *The Astrophysical Journal*, 752: 125.

Toner J. D., Catling D. C., and Light B. (2014) The formation of supercooled brines, viscous liquids, and low-temperature perchlorate glasses in aqueous solutions relevant to Mars. *Icarus*, 233: 36-47.

Tosca N. J., Knoll A. H., and McLennan S. M. (2008) Water activity and the challenge for life on early Mars. *Science*, 320: 1204-1207.

Trumbo S. K., Brown M. E., and Hand K. P. (2019) Sodium chloride on the surface of Europa. *Science advances*, 5: eaaw7123.

Turtle E. P., and Pierazzo E. (2001) Thickness of a Europan ice shell from impact crater simulations. *Science*, 294: 1326-1328.

USGS. (2000) Grains in an ice thin-section.

Vance S., and Goodman J. (2009) Oceanography of an ice-covered moon. *Europa*: 459-482.

Vance S. D., Barge L. M., Cardoso S., and Cartwright J. (2019) Self-Assembling Ice Membranes on Europa: Brinicle Properties, Field Examples, and Possible Energetic Systems in Icy Ocean Worlds. *Astrobiology*, 19: 685-695.

Vance S. D., Hand K. P., and Pappalardo R. T. (2016) Geophysical controls of chemical disequilibria in Europa. *Geophysical Research Letters*, 43: 4871-4879.

Vance S. D., Panning M. P., Stähler S., Cammarano F., Bills B. G., Tobie G., Kamata S., Kedar S., Sotin C., and Pike W. T. (2018) Geophysical investigations of habitability in ice-covered ocean worlds. *Journal of Geophysical Research: Planets*, 123: 180-205.

Vihma T. (2014) Effects of Arctic sea ice decline on weather and climate: A review. *Surveys in Geophysics*, 35: 1175-1214.

Waite J. H., Lewis W. S., Magee B. A., Lunine J. I., McKinnon W. B., Glein C. R., Mousis O., Young D. T., Brockwell T., Westlake J. and others. (2009) Liquid water on Enceladus from observations of ammonia and 40Ar in the plume. *Nature*, 460: 487-490.

Walker C. C., and Schmidt B. E. (2015) Ice collapse over trapped water bodies on Enceladus and Europa. *Geophysical Research Letters*, 42: 712-719.

Warren S. G., Roesler C. S., Morgan V. I., Brandt R. E., Goodwin I. D., and Allison I. (1993) Green icebergs formed by freezing of organic-rich seawater to the base of Antarctic ice shelves. *Journal of Geophysical Research: Oceans (1978–2012)*, 98: 6921-6928.

Weeks W. (2010) On sea ice. University of Alaska Press.

Weeks W. F., and Ackley S. F. (1986) The Growth, Structure, and Properties of Sea Ice. In: *CRREL Monograph*, U.S. Army Cold Regions Research and Engineering Laboratory, pp 9-164.

Weeks W. F., and Lofgren G. (1967) The effective solute distribution coefficient during the freezing of NaCl solutions. *Physics of snow and ice: Proceedings*, 1: 579-597.

Wells A. J., Hitchen J. R., and Parkinson J. R. G. (2019) Mushy-layer growth and convection, with application to sea ice. *Philosophical Transactions of the Royal Society A*, 377: 20180165.

Wettlaufer J. S. (1992) Directional Solidification of Salt Water: Deep and Shallow Cells. *Europhysics Letters (EPL)*, 19: 337-342.

Wettlaufer J. S. (1998) Introduction to crystallization phenomena in natural and artificial sea ice. *The Physics of ice covered seas, edited by: Lepparantä, M., Univ. of Helsinki, Helsinki*: 105-195.

Zimmer C., Khurana K. K., and Kivelson M. G. (2000) Subsurface Oceans on Europa and Callisto: Constraints from Galileo Magnetometer Observations. *Icarus*, 147: 329-347.

Zolotov M. Y. (2007) An oceanic composition on early and today's Enceladus. *Geophysical Research Letters*, 34.

Zolotov M. Y., and Kargel J. S. (2009) On the chemical composition of Europa’s icy shell, ocean, and underlying rocks. University of Arizona Press Tucson, AZ.

Zolotov M. Y., and Shock E. L. (2001) Composition and stability of salts on the surface of Europa and their oceanic origin. *Journal of Geophysical Research: Planets (1991–2012)*, 106: 32815-32827.

Zotikov I. A., Zagorodnov V. S., and Raikovsky J. V. (1980) Core Drilling Through the Ross Ice Shelf (Antarctica) Confirmed Basal Freezing. *Science*, 207: 1463-1465.